JIMMA UNIVERSITY

JIMMA INSTITUTE OF TECHNOLOGY

FACULTY Of MECHANICAL ENGINEERING

SUSTAINABLE ENERGY ENGINEERING CHAIR

Simulation and Experimental Evaluation of Solar Powered Egg Incubator with Integrated Thermal Energy Storage for Poultry Production:(Case Study: West Showa Zone Bako District, Ethiopia)

By

Duresa Tesfaye

A Research Paper Submitted to the School of Graduate studies of Jimma University in Partial Fulfillment of the Requirement for the Degree of Masters of Science in Sustainable Energy Engineering.

December 2021

Jimma, Ethiopia

JIMMA UNIVERSITY

JIMMA INSTITUTE OF TECHNOLOGY

FACULTY OF MECHANICAL ENGINEERING

SUSTAINABLE ENERGY ENGINEERING CHAIR

Simulation and experimental evaluation of solar-powered egg incubator with integrated thermal energy storage for poultry production: (Case study: West Showa Zone Bako District, Ethiopia)

A Research Proposal Submitted to the School of Graduate Studies of Jimma University in Partial Fulfillment of the Requirement for the Degree of Masters of Science in Sustainable Energy Engineering

Advisor: Prof. Ancha Venkata Ramayya (Ph.D.)

Co-Advisor: Mr. Fikru Gebre (MSc.)

December 2021

Jimma, Ethiopia

DECLARATION

I, the undersigned, declare that this research paper entitled" Simulation and experimental evaluation of solar egg incubator with integrated thermal energy storage for poultry production" is my original work carried out under the supervisors of Prof. Ancha Venkata Ramayya (PhD.) and Fikru Gebre (MSc.) and has not presented by any other person for an award of a degree in this or any other University.

Duresa Tesfaye (Candidate)

Sign_____________________ Date _________________

Approved By:

Advisor: Prof. A.Venkata Ramayya (PhD.)

Signature______________________ Date __________________

Co-advisor: Fikru Gebre (MSc.)

Signature______________________ Date__________________

External Examiner:____

Signature______________________ Date _________________

Internal Examiner: ____

Signature____________________ Date__________________

Chair: Terekegn Limore

Signature____________________ Date_________________

ACKNOWLEDGMENTS

Above all, I would like to express my deep sense of thanks to the Almighty God for giving me endurance, courage, and strength during this precise time and moment. I would like to express my gratitude to my Advisor Prof. A.Venkata Ramayya (PhD.) for allowing me to work on my thesis, as well as for your direction, support, and insightful remarks, without which this work would not have been accomplished. He has been a constant source of inspiration throughout my study period.

I am also grateful to my co-advisor Fikru Gebre (MSc.) for his kind help on different occasions. Besides my advisors, I would like to thank the Bako agricultural engineering research center process owner Mr. Gelgelo K. (MSc.) for his assistance, and encouragement according to this study.

Last but not least, I'd want to express my gratitude to all members and employees of the Mechanical Engineering faculty, at Jimma University Institute of Technology and BAERC, who assist me in various capacities/skills.

ABSTRACT

The sun's energy is the finest option for thermal energy generation because it is available all over the world and is free to use. Poultry egg incubation is requiring a continuous supply of energy for efficient performance and operation. On-grid power does not reach Ethiopia's rural areas, and even in those areas where it is available, electricity might be irregular or switched off at any time, causing incubators to malfunction, limited production, and expensive costs. The Use of generators increases the running cost of incubators and the Natural incubation process by hen produces a very small number of chickens. A solar-powered egg incubator with a thermal energy storage system was built, modeled, and tested in this study to assess its performance. A solar egg incubator was developed utilizing a solar collector with built-in sensible solid heat storage (placed below the absorber plate), a 50 eggs capacity incubation chamber, and a control unit. During the incubating period, there is sufficient sunlight that is converted into the energy required for a solar-powered egg incubator by a flat plate solar collector in the study area. The result showed that on the highest solar radiation days (629.3w/m^2) the average outlet collector temperature was 53^{o}C and 37^{o}C was obtained on the lowest solar radiation days (397.5w/m2). The maximum collector thermal efficiency was found to be 44.33 %. A total of 20 eggs were tested for both fertility and hatchability over 21-days in a solar-powered egg incubator. The incubating chamber was maintained by using a temperature controller (thermostat STC 1000) throughout the incubating period within a temperature range of 36.5 to 39.5 ^{o} C and a relative humidity range of 40 to 75 %. The percentage fertility and hatchability of eggs were 61.11% and 27.27 % respectively. In addition, the finite element (FE) model was developed using COMSOL Multiphysics 5.4 software to study the temperature distribution inside the solar collector. The lower extent of observable errors suggest a close match between the test and estimated interior solar collector temperature.

Key words: Collector, Incubator, Poultry, Performance, Sensible Storage**,** Solar Energy**.**

Table of Contents

LIST OF FIGURES

LIST OF TABLES

LIST OF ABBREVATION AND NOMENCLATURE

Abbreviations

BAERC	Bako agricultural engineering research
CSA	Central Statistical Agency
DNI	Direct Normal Irradiance
DNR	Direct Normal Radiation
EDC	Electricity Distribution Companies
FPSC	Flat-plate Solar Collector
ISO	International Standards Organization
NASA	National Aeronautics and Space Administration
NMSA	National Meteorological Service Agency
SEI	Solar Egg Incubator
TES	Integrated with Thermal Energy Storage
WMO	World Meteorological Organization

Nomenclature

Symbol	Meaning	SI Unit
$\dot{m}$	Mass flow rate	[kg/s]
C_{pa}	Specific heat capacity under constant pressure	[J/kg K]
h_c	Convection heat transfer coefficient	[W/m^2 K]
Ib	Average hourly Solar beam irradiation	[W/m^2]
Id	Average hourly Solar diffuse irradiation	[W/m^2]
Ig	Average hourly Global solar irradiation	[W/m^2]
k	Thermal conductivity	[W/mK]
L	Length	[m]
Q	Heat transfer rate	[W]
Q_{abs}	Absorbed heat	[W]
Q_L	Heat loss	[W]
Q_u	Useful heat	[W]
Re	Reynolds number	-
Ta	Ambient temperature	[K]
T_i	Inlet temperature	[K]
T_o	Output temperature	[K]
T_{sky}	Sky temperature	[K]
U_L	Heat loss coefficient	[W/m^{2}K]
V	Wind speed	[m/s]

η	Collector efficiency	[%]
ν	Kinematic viscosity	[m^2/s]
β	Coefficient of volumetric thermal expansion	[1/K]
α-	Absorbance	-
ε	Emittance	-
δ	Delta (declination angle)	[°]
τ	Transitivity	-
σ	Stefan Boltzmann constant	$[W/m^2K^4]$
ρ	Density	[kg/m^3]
N_u	Nusselt number	-
P_r	Prandtl number	-
Gr_L	Grashoff number	-
ϕ	Latitude	[°]
ω_s	Sunset hour angle	[°]
α	Soar altitude	[°]
ω	Omega (hour angle)	[°]
ε_g-	Glass emissivity	-
ε_p	Plate emissivity	-
ε_{eff}	Effective emissivity of plate-glazing	-
H_o	Monthly mean daily radiation on a horizontal surface in the absence of the atmosphere	
Ns	Monthly mean value of day length at a particular location,	

ns	Monthly mean daily number of hours of observed sunshine hours,	
h_w	Convection heat transfer coefficient between absorber and ambient air	[W/m^2 K
a, b	Climatologically determined regression constant.	
N	Number of days	

Subscripts

abs - Absorbed

a- Ambient

conv - Convection

In-Inlet

Out-Outlet

m- Mean

Loss-Losses

CHAPTER ONE

1. INTRODUCTION

1.1 Background of the Study

Egg incubators with regular, effective and efficient operation have the capacities of providing enough poultry chikens which can serve every household with sufficient amount of protein on daily basis. Incubation of egg is a process of transforming embryo in an egg into chick under favorable environmental condition with or without the consent of mother birds. There are two ways hatching of eggs can take place; one is by natural incubation which involves the broody bird sitting on a clutch of eggs while the other way is by artificial incubation which involves the use of incubator. The most important difference between natural and artificial incubation is that the parent provides warmth and stirring of the eggs by contact rather than surrounding the egg with warm air and provision of artificial stirrer.

A mother hen's bodily contact has a poor hatching efficiency, thus hatcheries use a technology that mimics the environmental conditions necessary for such an operation in an incubator to conduct this activity within the set temperature and ratio range[1]. These ranges are between 35.5-39^{o}C and 40–70% respectively. So to maintain this temperature range continuous heat supply is required[2]. The great majority of poultry farmers in agricultural regions in most developing countries run small-scale or even subsistence farms. They even use a group of bulb lamps and kerosene stoves to realize the heating requirements of the tiny hatcheries and brooders for day-old chicks. But the issues with these systems are enormous [3]. If we use fuel, it will produce toxic gases that are harmful to eggs and poultry. Egg incubators that operate on a regular, effective, and efficient basis can produce enough chicken birds to provide an adequate amount of protein to Ethiopian households regularly.

Artificial incubation is favored to extend the assembly of chicks and protein intake, particularly in developing countries. The electrical incubators are the most effective where the provision of electricity is instantly available and not cheap. But the provision of electricity is that the erratic, unreliable, and a high percentage of the population within the developing world isn't on the electricity grid. the choice, cheap, and readily available source of warmth should be provided for small-scale farmers involved in the production of chicks. Therefore, a solar-powered incubator integrated with a thermal energy storage system doesn't face this problem. It operates within the absence of power from the grid, it works from alternative energy, and that we need power from storage in extreme cases. Moreover, solar incubator makes employment opportunities for rural women also improve their lifestyle with free green energy.

1.2 Advantages of Using Solar Powered Egg Incubator.

Using solar-powered an egg in an incubator has positive advantages in the development of the country and the improvement of the living standard of the community. Thus, a solar-powered egg incubator will:

- Improve household incomes - through making job opportunities for rural women.
- Protect the environment (global warming) due to the transition to cleaner energy sources.

1.3 Incubation Technology

Depending upon the energy input to the incubator, an egg incubation technology is broadly classified into four:

(i) Electrical incubators
(ii) Kerosene stove incubators
(iii) Gas incubators
(iv) Solar incubators, etc.

The electrical incubator: is an automated machine that utilizes electrical energy supply from the mains by the Electricity Distribution Companies (EDC). This source of energy is presently erratic and unreliable for use in the electrical incubator which will have to run on the mains supply for 21 days[4].

The kerosene stove is a type of incubator that runs on kerosene heat for the whole 21-day incubation period. And, because of the excessive cost of liquid fuels, this method of producing day-old chicks has proven to be an extremely costly endeavor. Due to the high cost of liquefied gas, incubation is not a cheap enterprise.

An alternative source of heat for the incubation of day-old chicks is the energy supply from Biomass sources such as animal waste, municipal solid waste, agricultural waste, and industrial waste, which produces energy in the form of combustible gas known as biogas. This has no undesirable effects on the environment. This form of energy could be used directly for the supply of heat to the incubator for the whole period of incubation of chicken eggs adequately. The synthesis of biogas is principal, methane (50-70%), carbon dioxide (30-40%), and the rest is comprised of hints of components like hydrogen, nitrogen, and hydro-sulfide [5].

The only popular existing incubator that is cheap based on the readily available source of heat is the solar-type incubator which requires to be manned by highly skilled and technically knowledgeable personnel. This will equally add to the cost of the day-old chicks due to its initial capital cost.

1.4 Statement of Problems

Poultry egg incubation is an activity that requires a continuous supply of energy for efficient performance and operation. Electricity-based egg incubators are recognized to provide clean energy with minimal environmental impact, but their use is limited caused by frequent power cuts in areas where grid electricity is available. And thus, it becomes a dream for people in rural areas to get into poultry farms. The Outage of power affects the temperature and humidity of incubation leading to reduced hatchability and impairs the operation of the incubators, which reduces their level of performance, low creation, and significant expense of poultry chicken. Naturally, the egg hatching process is completed by a broody mother hen, but it has limitations in terms of egg hatching capacity, care of mother hen, weather, and other mother mistakes. The usage of generators drives up the cost of running incubators, making day-old chicks prohibitively expensive. The best alternative is to use a different energy source, such as solar thermal power. That is why the proposed solar-powered poultry egg incubator comes into play. It can operate in the absence of power from a grid, it works from -solar power and we need power from grid or battery only in extreme cases.

1.5 Objective

1.5.1Main objective

The main objective of this research is to simulate and make an experimental evaluation of a solar-powered egg incubator with integrated built-in sensible thermal energy storage for poultry production.

1.5.2 Specific objectives

The Specific objectives of the research are :

- To estimate solar energy potential of the study area
- To Construct a prototype of a solar-powered egg incubator integrated with thermal energy storage to conduct experiment
- To Carry out performance analysis of flat plate solar collector for this study area through COMSOL software
- To Validate the performance of simulation by experimental verification

1.6 Scope of the Study

This work is concerned with simulation and experimental evaluation of the solar-powered egg incubator integrated with thermal energy storage for the study area. In this research, assessing the available solar potential for the study area, the system thermal analysis, COMSOL simulation, and system prototype construction were done. The experimental test was conducted under normal environmental conditions of the study area. Finally, the performance of an egg incubator integrated with sensible thermal energy storage was studied, the study only focuses on the incubator temperature and humidity (physical test). However, the cost analysis and the growth of the fertile and hatchability of the egg were not performed.

1.7 Significance of the Study

The experimental findings have the potential to support the deployment of a solar egg incubator (SEI) in conjunction with a thermal energy storage (TES) system. The study could be considered as a first for study area for thermal energy storage energy utilization technology to egg incubation, which is the better solution to the energy problem available in the study areas of the community. The use of solar energy for chicken production was a major advantage of this study. To create a good atmosphere of the environment by using flat plate solar collector systems rather than use kerosene as a power source

- ✓ to use as a reference for further analysis of the study area, and Areas or sectors including smaller households that need to use a solar-powered egg incubator and researchers are the beneficiaries of this technology
- ✓ To create awareness for other poultry producer areas, which have solar energy potential to adopt such technologies

CHAPTER TWO

2. LITERATURE REVIEW

Numerous types of egg incubators were designed and developed by various researchers, by using several different sources of energy. An incubator could be mainly used for five types of energy sources; electrical, biogas, solid fuel (charcoal), fossil oil (kerosene or gas, diesel-based generator), or solar types based on the source of energy[6]. While the various types of egg incubators used types of energy sources have their merits and limitations [7]. The incubators having solid fuel, fossil, oil, or biogas as their source of heat generate soot and other combustion products show that the lower percentage of hatchability of eggs[6]. Chipped away at extending domesticated animals' creation in Nigeria, including the advancement of savvy bird-egg hatchery models. In their model, which included the use of still air and oil lamps as sources of heat for the egg incubator, they found that the still-air incubator is the most time-consuming, with a hatchability rate of 33% [8].

According to the accomplished work on development and evaluation of a passive solar-powered system for poultry egg Incubation' electricity supply in developing counties like Nigeria has remained inadequate and unreliable alternative methods of meeting the energy needs in agriculture and also the poultry industry specifically[9].

Some groups of researchers Performed work on a thermal storage solution and they harvested solar energy using solar collectors to power incubators [10]. As properly as they mentioned that there's a disadvantage the usage of solar thermal collectors, warm water, air, oil, or different flowing materials, and that heated cloth can't without a doubt be placed right into a battery, not like the power generated via way of means of a solar panel can do. The problem along with his system is how the thermal storage unit would be able to store and release the warmth when the sunset and particularly on days when the sun is hidden behind clouds.

Kelleh Gbawuru Mansaray meted out, Fabrication and performance of a solar energy egg incubator, the solar photovoltaic powered chicken egg incubator was designed, fabricated, and tested to gauge its performance[11]. the key components are incubating unit, temperature device, and solar PV system. The incubating unit was generally maintained throughout the incubating temperature range of 36.8-37.9 degrees Celsius and **a** mean relativity humidity of 67.3%. Many variables could have contributed to the low hatchability rate, including cloudy weather, poor egg storage, time and energy spent flipping eggs, defective eggs, and so on. The research carried out on the 'Development of solar collectors combined with thermoelectric modules for solar drying technology has been successfully developed, analyzed, and see-beck effect is applied [12]. It means that the heat energy is converted directly into electricity. The goal of this study is to develop a sun drying technology that incorporates a solar collector and a thermoelectric generator module (TEG). Solar collectors can be the operator and produce hot air temperatures of about 70-80degree Celsius. The common bottom temperature of the collector is 45.4 Celsius, in which the ambient temperature becomes 35.4 Celsius, in regions with snow or no sunshine, masses of clouds or tree corners, dusty floral, etc.

The study on performance evaluation of monocrystalline photovoltaic panels in FUNAAB, Alabata, and Ogun State, Nigeria weather condition was carried out and this study recommended that performance test must be carried out on the solar panels whenever it's to be used to power any load (egg incubator) to ensure that the provide solar PV solar panel would be able to produce the power required to power the load (egg incubator) without failing [13].

Table 2. 1 Summary of the review of various incubator technologies

S/ no	NAME OF RESEARCHER'S	INCUBATOR TECHNOLOGY USED	SUMMARY OF THE RESEARCH
1	Adewunmi & Falayi.	solid fuel, fossil, oil, or biogas	The result comes from using those types of energy sources are Very low of an egg hatchability
2	Agboola et al.	Oil lamp	Performed work on increasing livestock production they indicated that the still-air incubator is the most tedious process and, in the model, they obtained 33 % of the success rate of hatchability.
3	Ahiaba	Passive solar	Identify electricity supply in a developing country has remained inadequate and unreliable alternative methods of meeting the energy needs in agriculture and the poultry industry specifically
4	Graham et al.	Solar with thermal energy	The problem with his system is how the thermal storage unit would be able to store and release the heat.
5	Kelleh G. Mansaray	Solar power	The low hatchability rate could have resulted from many factors including overcast weather, poor storage of eggs, time and energy wasted in turning eggs, faulty eggs etc.

6	S. Thongsan and et-al	Solar collector combined with thermoelectric	Solar collectors can be an operator and produce hot air temperatures of about 70-80degree Celsius. The average backside temperature of the collector was 45.4 degrees Celsius, whereas the ambient temperature was 35.8 degrees Celsius
7	Osanyinepeju et al.	Solar PV cell	recommended that performance tests must be carried out on the solar panels whenever it's to be used to power any load (egg incubator).

Almost in all literature reviews presented, the researchers expend their effort on the design and modeling as well as on the performance evaluation of different types of incubators, However, only a few of them deal with the solar integrated thermal energy storage for an egg incubator and efficient use of energy in the system. Thus, in this research, the researcher aimed to simulate and make an experimental analysis of solar-powered egg incubators with integrated thermal energy storage and provide for the community. This will reduce the energy bill and help to use. In addition to that, it will reduce the load from the national grid and increase the need for a community to use clean energy for almost all applications of incubation.

CHAPTER THREE

3. METHODS AND MATERIALS

3.1 Description of Experimental Site

The experiment was carried out at the Bako agricultural research center, which is located 250 kilometers west of Ethiopia's capital city, Addis Ababa. Specifically, it is located at geographical coordinate 9°06' N-latitude, 37°09' E -longitude, and at an altitude of 1650m above mean sea level with a total population based on the central statistical agency of Ethiopia (CSA) is about 184,925 in 2017 GC.

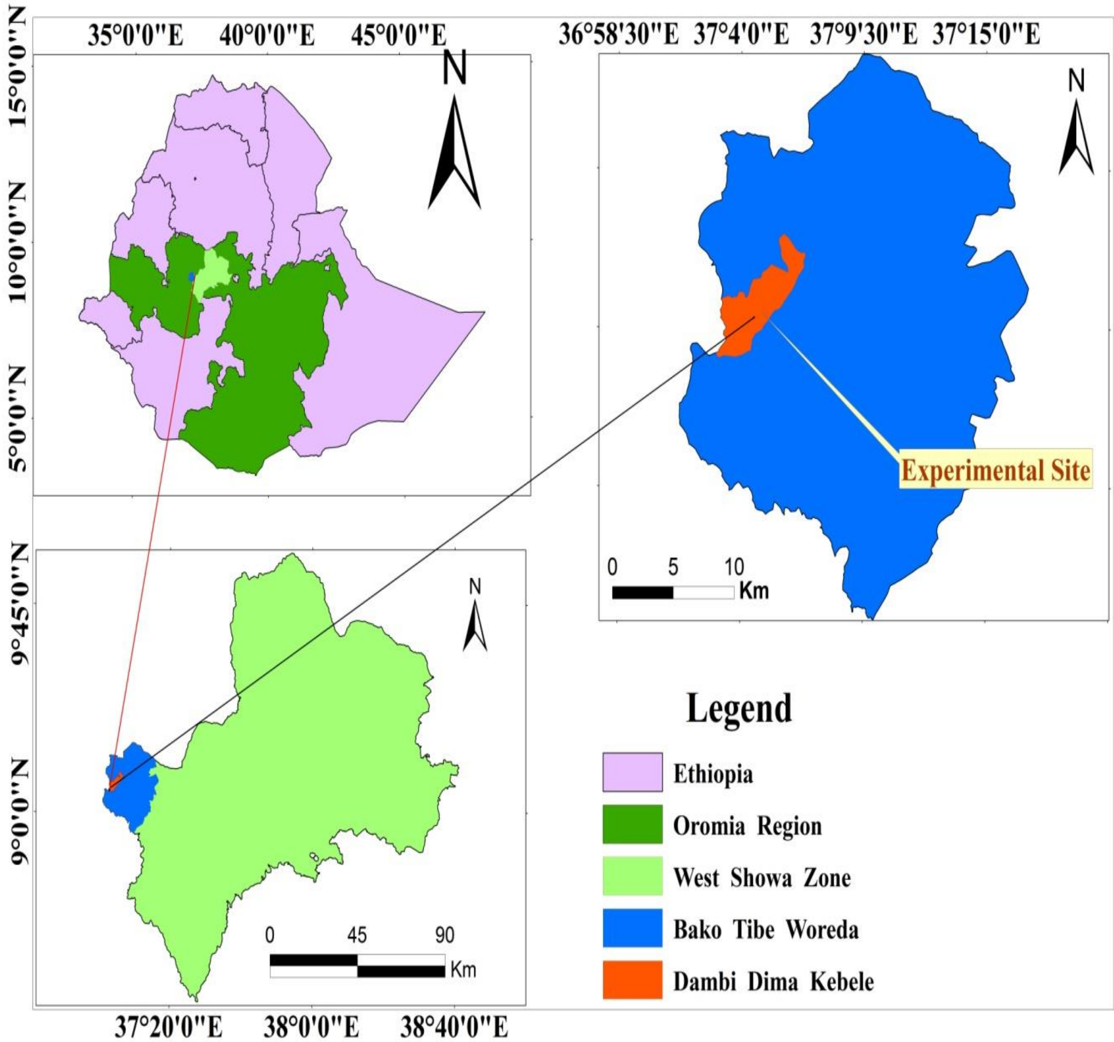

Figure 3. 1 Map of Study Area (GIS map)

3.2 Methodology

This study was conducted to simulate and experimentally evaluate an incubator that uses solar energy and integrates thermal energy storage for poultry production, to achieve the objective of this work, surveying the literature from related work, referring to the journals, books, and other unpublished material that were conducted. The estimation of solar data, analysis of the main components and the system description, System simulation, manufacturing, and direct solar radiation measurement during an experimental test were done. To estimate the available solar radiation for the study location MATLAB software was used and the solar data used for the estimation of the solar potential were collected from three different meteorological stations. Those are the National Meteorology Agency of Bako agricultural research center station (NMAS), Solar and wind energy resource assessment (SWERA website), and NASA Surface meteorology. From each meteorological agency, the last 5 years' averages of solar data were taken at Latitude 9.06/Longitude 37.09 and Elevation 1650m. The system was modeled by using COMSOL-multiphysics software system to analyze at reference meteorological conditions of Bako agricultural research center meteorological station. This software was chosen over other similar software for its simplicity and flexibility. The experimental test was performed under normal weather conditions at Bako agricultural engineering research center and the result was evaluated. The overall techniques and procedures were applied to achieve the specific objectives of this study are shown in the figure below

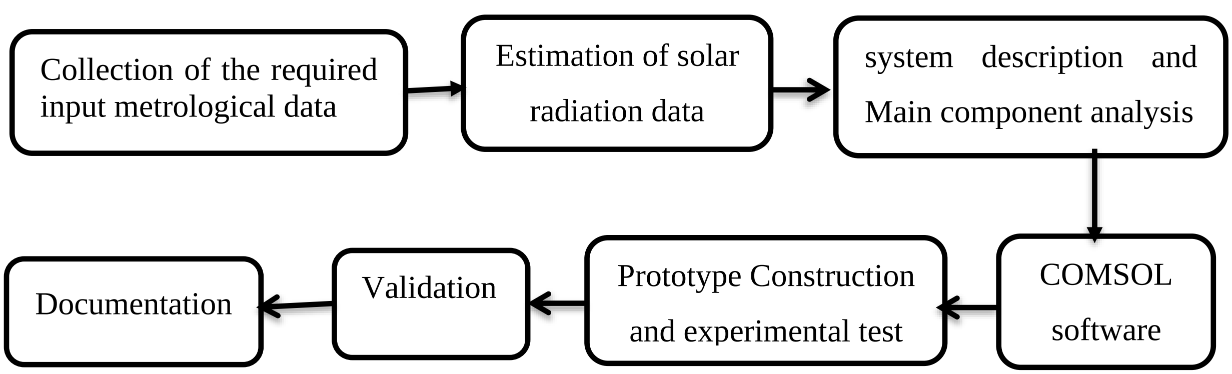

Figure 3. 2 Procedures and techniques used

3.3. Estimation of Solar Radiation of the Study Area

Solar radiation is the amount of available solar energy on the ground surface over a specified time, expressed as kWh/m^2 or MJ/m^2 and Solar radiation data is necessary for any solar conversion device design and to determine the level of solar radiation at a given location and the amount of energy available at various orientations of the collector. The most detailed information available is beam and diffuse radiation on a level that is helpful in simulations of solar processes [14]. In non-industrial nations like Ethiopia, in light of the nonappearance or glitch of estimating instruments, solar radiation information isn't accessible. However, lacking these data from meteorological locations, it is possible to use empirical relationships to predict solar radiation from hours of sunshine. Data on average sunlight hours or the average percentage of available sunshine hours may be obtained from a variety of meteorological stations around the nation. The following table shows that the meteorological data recorded from the National Meteorology Agency of Bako agricultural research center station.

Table 3. 1 Monthly average given (input) parameters

Month	Sun hours(hr)	Mean day	Ta(ºC)	Humidity (%)	Wind (km/day)
January	8.5	17	21.25	51	73
February	8.6	47	22.05	48	82
March	7.9	75	22.6	48	94
April	7.4	105	22.9	51	30.4
May	7.1	135	22	57	31.4
June	5.8	162	20.5	66	31.2
July	3.6	198	19.7	72	31.3
August	3.4	228	19.5	72	29.2
September	4.7	258	20	70	26.2
October	7.5	288	20.65	63	24.5
November	8.7	318	20.6	58	24.3
December	8.9	344	20.5	54	25.4
Average	6.8		22	59	27.7

3.3.1 Estimation of monthly average daily global radiation

The principal exact relationship utilizing the prospect of utilizing daylight hours for the assessment of overall radiation was proposed by Angstrom. The Angstrom correlation was modified by Prescott and Page. the best model accustomed estimate monthly average daily radiation on a level is that the well-known Angstrom correlation which can be given by equation (3.1) [15]

$$\frac{H}{HO} = a + b(\frac{ns}{Ns}) \quad (3.1)$$

a, b – empirical constants, (Values are obtained by regression).

The relapse coefficients "a" and "b" are relied upon to improve by adding the impact of rising, daylight length, and scope together. In this manner, the relapse coefficients "a" and "b" as far as the scope, height, and level of conceivable daylight for any area throughout the Planet (for 5°< Φ <54°) are connected by Gopinathan with the situation underneath:

$$a = -0.309 + 0.539cos\phi - 0.0693h + 0.29(\frac{ns}{Ns}) \quad (3.2)$$

$$b = 1.529 - 1.027cos\phi + 0.0926h - 0.359(\frac{ns}{Ns}) \quad (3.3)$$

Where: *H* -Monthly average daily radiation on the horizontal surface.

H_O- Monthly average radiation outside of the atmosphere (ETR on the horizontal surface) for the same location

*n*s- Monthly average daily hours of bright sunshine.

Ns- Monthly average of the maximum possible daily hours of bright sunshine

For this study, the data taken from site measurement with GPS gives as:

Elevation(h)=1650 =1.65km, and ϕ =9.06

Declination Angle

Declination is the angle between the equator plane and a line drawn from the earth's center to the sun's center at solar noon (i.e., when the sun is on the local meridian) for respect to the plane of the equator (e.g., the angle between the equator plane and a line drawn from the earth's center to the sun's center)[14]. The angular position of the sun at solar noon (i.e., When the sun is on the local meridian) concern for the plane of the equator, north positive; $-23.45^\circ \leq \delta \leq 23.45^\circ$. Its value in degrees for n, an average number of the days in the month (Table 3.2) is given by Cooper's equation:

$$\delta = 23.45 \sin\left[360 * \frac{284+n}{365}\right] \quad (3.4)$$

where an angle is in degrees (^{0}) and n is the day of the year, numbering from January 1

Table 3. 2 Recommended Average Days for Months and Values of n by Months [14]

Months	***No. of day for The i^th^ day of the month***	***For the average day of the month***		
		Date	***Day of year(nd)***	***Declination (δ)***
January	i	17	17	-20.92
February	31+i	16	47	-12.95
March	59+i	16	75	-2.42
April	90+i	15	105	9.41
May	120+i	15	135	18.79
June	151+i	11	162	23.09
July	181+i	17	198	21.18
August	220+i	16	228	13.45
September	243+i	15	258	2.22
October	273+i	15	288	-9.60
November	304+i	14	318	-18.91
December	334+i	10	344	-23.05

The sun declination angle for all twelve months is calculated as follows. The average values should be taken at the first and end of the month.

For January the maximum and minimum values and their average value is calculated below

At the 1st of the month n= 1

$$\delta = 23.45 \sin\left[360 * \frac{284+n}{365}\right] = -23.0116\,^{o} \text{ at } n = 1$$

$$\textit{at the end of the month } n=31$$

$$\delta = 23.45 \sin\left[360 * \frac{284+n}{365}\right] = -17.78\,^{o}$$

For all remaining months, the values are found in the same way as above.

Sunset Hour Angle

The sunset hour angle in degree, ωs can be calculated by using equation (3.5) and the values for each month of the year are tabulated in Table 3.2 for the study location.

$$\omega s = cos^{-1}(-tan\phi tan\delta) \qquad (3.5)$$

Estimating Sunrise and Sunset hours knowing the local latitude (ϕ), the sun's declination (δ), and the solar time correction that is used to calculate the time of sunrise and sunset hours.

Table 3. 3 Sunset hour angle of the location

Sunset Hour Angle (ωs)											
Jan	Feb	Mar	Apr	May	Jun	Jul	Aug	Sep	Oct	Nov	Dec
86.53	87.91	89.61	91.5	93.1	93.87	93.51	92.16	90.35	88.47	86.89	86.14

Sunshine Duration

The monthly mean value maximum possible sunshine hour of day length (Ns) at a particular location calculated by using Cooper's formula:

$$Ns = \frac{2}{15^0} * \omega s \qquad (3.6)$$

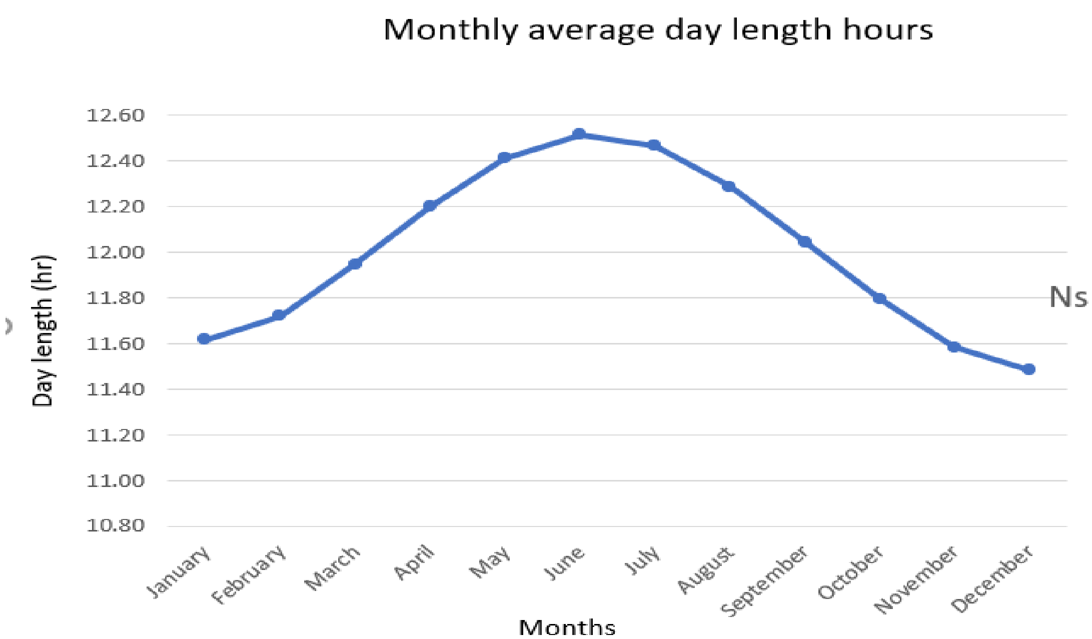

Figure 3. 3 Day length hours

Extraterrestrial Radiation

The monthly average radiation outside of the atmosphere (extraterrestrial radiation on a horizontal surface) HO calculated as:

$$Ho = \frac{24*3600}{\pi} * Gsc[(1 + 0.033\cos\left(360 * \frac{n}{365}\right)] \; [\cos\phi \cos\delta \sin\omega s + \frac{\pi}{180} * \sin\delta sin\phi] \quad (3.7)$$

Where: ωs= sunrise hour angle

Ho -in *W h/ m² /day*

Gsc -1367 *W* / *m²* (Solar constant)

Where: *n is* recommended average days for the month

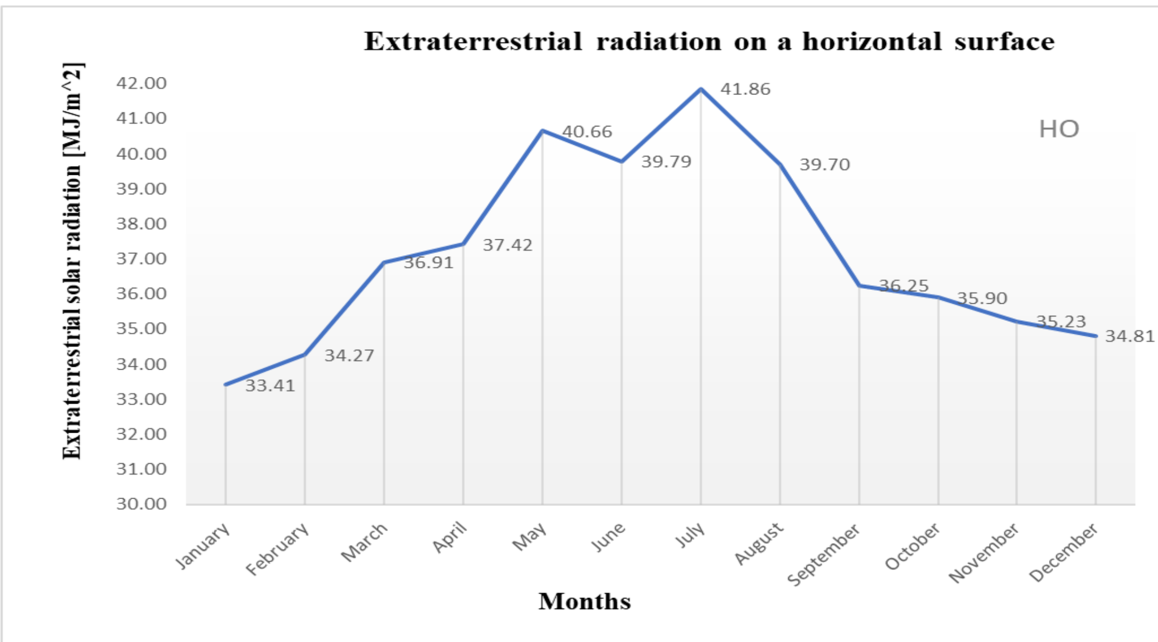

Figure 3. 4 Extraterrestrial radiation on a horizontal surface

3.3.2 Estimation of monthly average daily diffuse radiation

Average daily diffuse irradiance over a horizontal surface can be determined from the monthly average global irradiance over the horizontal surface and the number of hours of bright sunlight[15].

$$\frac{Hd}{H} = 0.931 - 0.814\left(\frac{ns}{Ns}\right) \quad (3.8)$$

Where H_d = Diffuse radiation

3.3.3 Estimation of monthly average hourly global radiation

The monthly average hourly global radiation in the horizontal plane can be calculated based on the knowledge of the monthly average daily global radiation in the horizontal plane [15].

$$\frac{Ig}{H} = \frac{\pi}{24}(a + b\cos\omega))\frac{\cos\omega - \cos\omega s}{\sin\omega s - \frac{\pi}{180}\omega s\cos\omega s} \ldots\ldots\ldots\ldots\ldots\ldots\ldots\ldots (3.9)$$

Where: Ig is monthly average hourly global radiation and ω is the hour angle in degrees for the time under the study given by equation (3.12) and the coefficients a and b are expressed as:

Were, $a = 0.409 + 0.5016\,sin(\omega s - 60) \ldots\ldots\ldots\ldots\ldots\ldots\ldots\ldots (3.10)$

$$b = 0.6609 - 0.4767\,(\omega s - 60) \ldots\ldots\ldots\ldots\ldots\ldots\ldots\ldots (3.11)$$

Hour Angle; Is the angular displacement of the sun east or west of the local meridian due to the rotation of the earth on its axis. The hour angle increases by 15^{O}every hour; morning negative, afternoon positive. Mathematically Hour angle ω and solar time ST in hours are related as;

ω=15 (LTS-12) ……………………………………………………………. (3.12)

Where LST = local solar time.

In Bako Tibbe and nearest to it the maximum temperature occurs averagely from 5 (11) to 9 (15) o'clock. The hour angle at these times from definition is calculated as follows:

For 5(11) LST = 5(11)

ω=15 (LST−12) ω=15 (11−12) =-15 ^{o}

3.3.4 Estimation of monthly average hourly diffuse radiation

The monthly average hourly diffuse radiation in the horizontal plane can be calculated based on the knowledge of the monthly average daily diffuse radiation in the horizontal plane [15].

$$\frac{I_d}{H_d} = (\pi/24\frac{\cos\omega - \cos\omega s}{\sin\omega s - \frac{\pi}{180}\omega s\cos\omega}) \ldots\ldots\ldots\ldots\ldots\ldots\ldots\ldots (3.13)$$

Where I_d =monthly average hourly diffuse radiation

The ratio of average hourly total to daily total radiation as a function of hour relative to solar noon and the day length. The number of days is assumed to be symmetric concerning solar noon and the time represented by its midpoint. In the present study, the monthly average hourly horizontal global and diffuse radiation for the given sunshine hours of Bako Tibbe was also calculated.

3.4 Description of the System

Figure 3.6 shows a schematic diagram of a solar-powered egg incubator integrated with a thermal energy storage system considered. The main components of the system are the incubating unit, flat plate solar collector with built-in thermal energy storage system, and temperature control device set (thermostat set). Incubating cabinet was made up of 2 mm thick galvanized sheet metal, lined at the edge with plywood. The external length, width, and height of the outer box are 50 cm, 50 cm, and 57 cm respectively, the space between the inner box and outer box is filled with straw foam to reduce heat losses.

The incubator's door was built of comparable materials. The inside (incubating chamber) has egg trays and holders with a forward and back mechanism, as well as an evaporative moisture pan to regulate relative humidity. The heat source for incubation is hot air from the solar collector into the chamber. For the collector, the casing was made of plywood and the inner box was constructed using 2mm aluminum thick painted black to increase its absorption. A fiberglass substance fills the area between the outer box and the inner box was about 40 mm thick to reduce heat losses . The airflow channel (upper compartment) is located between the absorber plate and the transparent top cover, while the thermal storage unit (lower compartment) is located between the absorber plate and the backplate. The overall length, width, and height of the solar collector are 1200 mm, 680 mm. and 250 mm respectively. The collector top glazing is a single-layer transparent glass sheet of 4 mm in thickness.

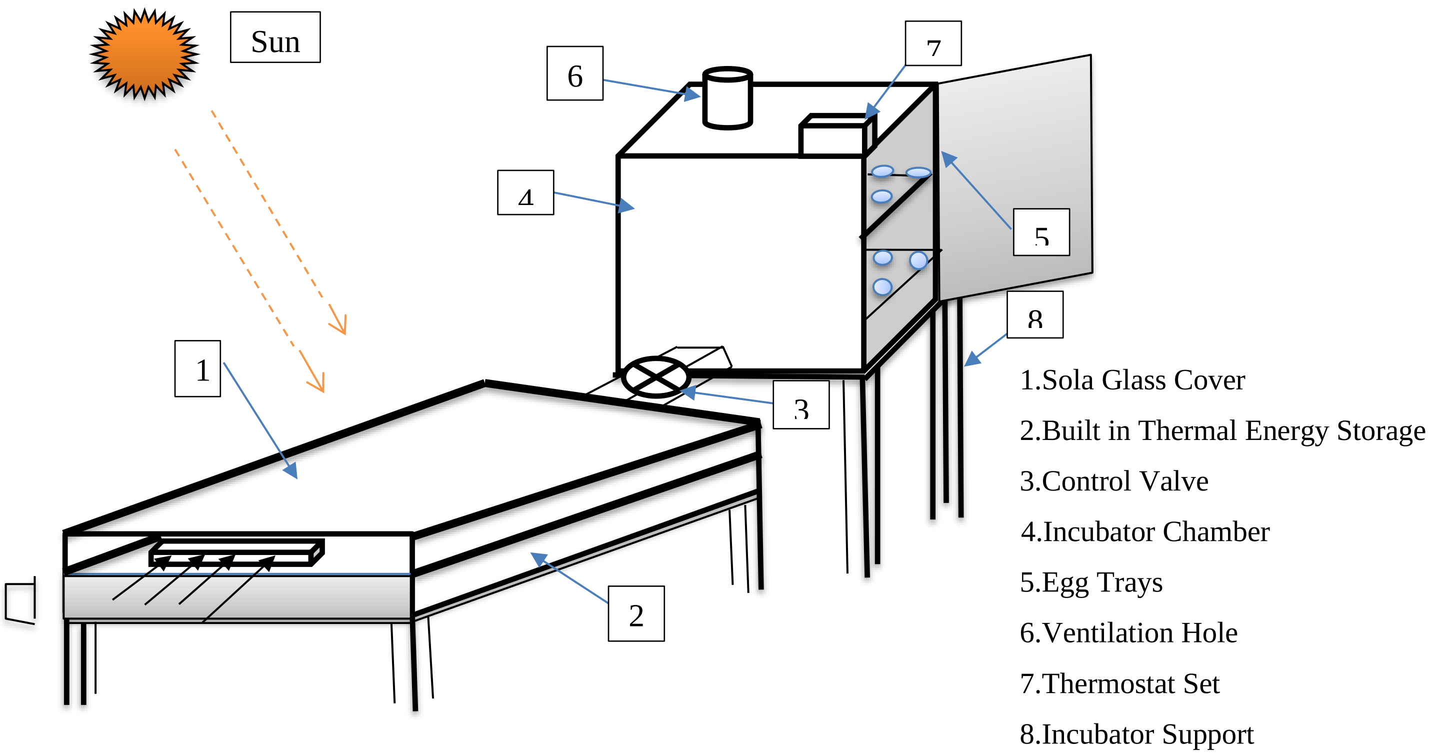

Figure 3. 5 A schematic diagram of a solar-powered egg incubator system studied

The thermal storage contains rock pebbles of 145.5 kg. The heat absorbed by the absorber plate is partially transferred to the air passing through the collector in the top compartment and partially transferred to the loosely packed heat-absorbing pebbles in the bottom compartment (storage unit). Because the absorber plate is the source of heat for the rock pebbles, it is constantly hotter than the pebbles during sunlight hours. During this time, the rock pebbles are getting charged. The energy stored in the rock pebbles is released and transmitted via the absorber plate to the air flowing through the collector during off-sunshine hours when the absorber plate is absorbing little or no energy.

3.5 Flat-Plate Solar Collector

Solar collectors are used to converting direct and diffuse radiation from the sun into thermal energy. it's a special quite device that transforms alternative energy to heat. Energy is moved from an abroad wellspring of energy to a liquid.

Level plate gatherers might be intended for applications requiring energy conveyance at moderate temperatures, up to maybe 100°C above the surrounding temperature. They use both beam and diffuse radiation, don't require tracking of the sun, require little maintenance, and that they are mechanically simpler than concentrating collectors[16]. Generally, flat plate collector designs encompass three major parts. These are transparent glass cover, absorber plate, and insulation. The transparent cover also called glazing is where the solar power passes through the collector. Glass is that the common transparent protect collector, the absorber plate is formed from a fabric that might rapidly absorb heat from the sun's rays. it's usually made of black painted metal sheet. Insulation should be used at the rear side of the absorber to attenuate heat loss.

3.6 Energy gained by the solar collector

The energy gained by the solar collector can be expressed by the following relation[15]:

$$Qu = \tau\alpha It\, Ac - U_L\, A c\, (Tc - Ta) \quad (3.14)$$

Where, Ac = area of transparent cover (m^2)

I_t = total incident radiation on the collector surface ($W.\ m^{-2}$)

U_L = overall heat loss for the collector ($W.\ m^{-2}.K^{-1}$)

α = solar absorptance

τ = transmittance

T_c = collector temperature (K)

Ta = ambient air temperature (K)

3.6.1 Overall loss coefficient and heat transfer correlations

According to an insightful perspective, it is helpful to utilize the complete misfortune coefficient characterized by the recipe to communicate the warmth misfortune from the authority.

$$Q_L = U_L\, A_c(T_{pm} - T_a) \quad (3.15)$$

Where T_{pm}- the average temperature of the absorber plate

The heat lost from the collector is the sum of the heat lost from the top, the bottom, and the sides. Thus,

$$Q_L = Q_{b+} Q_{t+} Q_s \quad (3.16)$$

Each of these losses is also expressed in terms of coefficients called the top loss coefficient, the bottom loss coefficient, and the side loss coefficient

3.6.1.1Top loss coefficient

The upper misfortune coefficient Ut is assessed by considering the convection and re-radiation loss of the assimilation plate the vertical way. It is assumed that the temperature drop in the thickness of the roof is negligible, and the interaction between the incident solar radiation absorbed by the roof and the emission loss is negligible. The outgoing re-radiation is long-wavelength. For these wavelengths, the transparent cover will be assumed to be almost opaque.

$$U_t = \left(\frac{1}{h_{c,p-g} - h_{r,p-g}} + \frac{1}{h_w - h_{r,g-amb}}\right)^{-1} \quad (3.17)$$

Based on the maximum plate temperature is 73°C and cover glass temperature is 43°C. The mean temperature between them is 58° C, so the air properties on this temperature: the property of air at 58 ° C are not available on-air property table so it was calculated by interpolation. The value obtained was:

ρ (density of air) = 1.065kg/m^3

Cp (specific heat of air) = 1007KJ/kg*k

K (thermal conductivity) = 0.027934w/m*k

α (thermal diffusivity) = 2.503*10^{-5} m^2/s

ν (kinematic viscosity) = 1.876 *10^{-5}m^2/s

μ (dynamic viscosity) = 1.988*10^{-5} kg/m.s

pr (Prandtl number) = 0.72

A) Radiative Heat Transfer Coefficient

i)From the plate to the cover

The radiative heat transfer coefficient from the plate to the glass cover is expressed as:

$$h_{r,p-g} = \frac{\sigma\left[(T_P+273)^2+\left(T_g+273\right)^2\right][(T_P+273)+(T_g+273)}{[\frac{1}{\varepsilon\rho}+\frac{1}{\varepsilon g}-1]} \quad (3.18)$$

$$\varepsilon_{eff} = \left(\frac{1}{\varepsilon\rho} + \frac{1}{\varepsilon g} - 1\right)^{-1} \quad (3.19)$$

$$h_{r,p-g} = \frac{5.669*10^{-8}(346^2+316^2)(346+316)}{\frac{1}{0.84}+\frac{1}{0.95}-1} == 6.64\ w/m^2k$$

ii) From cover to the ambient

The effective temperature of the sky is usually calculated from the following simple empirical relation in whom temperatures are expressed in Kelvin

$$T_{sky} = T_{amb} - 6 \quad (3.20)$$

The radiative heat transfer coefficient from the glass cover to the ambient is expressed as:

$$h_{r,g-amb} = \frac{\sigma\varepsilon g(T_g+273)^4-(T_{sky}+273)^4}{(T_g-T_{amb})} \ldots\ldots\ldots\ldots\ldots\ldots\ldots \text{(3.21)}$$

$$= 5.01w/m^2k$$

B) **Convective Heat Transfer Coefficient**

i)From the plate to the cover: The natural convection heat transfer coefficient h_{1c} is related to three dimensionless parameters, the Nusselt number Nu, the Rayleigh number Ra, and the Prandtl number Pr, that are given by:

$$Nu = \frac{hL}{K} \qquad Ra = g\beta\left(\frac{\Delta T}{v\alpha}\right)L^3 \qquad pr = v/\alpha \ldots\ldots\ldots\ldots \text{(3.22)}$$

h- heat transfer coefficient [W/m^2 K]

L – is the plate spacing, (0.35)

g – The gravitational constant,

ΔT – Temperature difference between the plate and the glass, and

β– is the volumetric coefficient of expansion of air.

$$Ra = g\beta\left(\frac{\Delta T}{v\alpha}\right)L^3$$

$$Ra = 9.81 * \frac{30 * 0.72 * 0.035^3}{2.503 * 1.876 * 10^{-10}} = 333334$$

The convective heat transfer coefficient is,

$$N_u=0.54*Ra^{0.25}$$

$$Nu=0.54*333334^{0.25}$$

$$Nu=12.97$$

$$h_{c,p-g}= Nu * \frac{k}{L}=12.97*0.0278/0.055$$

$$=6.56w/m^2k$$

Wind heat transfer coefficient is given as (Watmuff, Charters, and Proctor 1977)

$$h_w = 2.8 + 3v \ldots\ldots\ldots\ldots\ldots\ldots\ldots\ldots\ldots \text{(3.23)}$$

$$h_w = 3.04$$

Where, ν is the average velocity of air at the inlet, for Bako, v=0.08m/s

$$U_t= \left(\frac{1}{h_{c,p-g}+h_{r,p-g}} + \frac{1}{h_w+h_{r,g-amb}}\right)^{-1}$$

$$U_t= \left(\frac{1}{6.56+10.8} + \frac{1}{3.04+7.92}\right)^{-1} = 6.71w/m^2k$$

3.6.1.2 Bottom heat loss coefficient

Assume that the heat flow is one-dimensional and stable. In most cases, the thickness of the insulation provided causes conduction-related thermal resistance to dominate. Therefore, ignore the resistance to convection at the bottom of the collector casing:

$$U_b = \frac{Ki}{\delta i} \quad \text{...} \quad (3.24)$$

where Ki - thermal conductivity of the insulation

δb - back insulation thickness

$$U_b = 1.07 w/m^2 k$$

3.6.1.3 Side loss coefficient

As on account of the base misfortune coefficient, it was accepted that the conduction obstruction overwhelms and that the progression of warmth is one-dimensional and consistent.

$$U_s = \frac{A1Ki}{Ac\delta e} \quad \text{...} \quad (3.25)$$

U_S= 3.68*0.043/0.816*0.04=4.8w/m^2k

Where: A_1- P*d_e =3.68m^2

P – the perimeter of the absorber plate. (m)

de – the height of the edge. (0.64m)

δe - an edge insulation thickness. (0.04m)

Overall heat coefficient

The overall heat loss coefficient U_L is the sum of the top, bottom, and edge loss coefficients.

That is: $U = U_t + U_b + U_s$ = $6.7 + 1.075 + 4.8 = 12.02w$

Over all heat loss

Assume ; mean temperature of collector 43^{o}C and mean air temperatue is 22^{o}C

Q_L=12.02(43-22) = 252w

Where, Ta = air temperature and Tm = mean temperature of the collector

According to metrological data, the annual average daily radiation in an area reaching the ground is; E=6.01kwh//m^2/day*day/6h=995w/m^2

To change E into w/m^2 average sunshine hour 6 hr. One part of the heat is transmitted due to cover glass and absorptive surface material selection for cover glass is Plexiglas

τ= 0.8 and $\propto$ =0.95

Qu= $\propto\tau$ E= 0.95×0.8×995 w/m^2 =794w/m^2

q_{opt} = E−Q_a = 995w/m^2 – 794w/m^2 = 201 w/m^2

Usable heat derived from the collector

Qu = α. τ. E- k [Tm-Ta] …………………...………………………………… (3.26)

Qu = 542w

The thermal efficiency of the collector is defined as the ratio of useful energy gain by the air to the solar radiation incident on the absorber of the solar collector[6]

$$\eta = \frac{Qu}{I_t A_c} \quad (3.27)$$

$$\eta_{th} = \frac{542}{995*0.816} = 44.33\%$$

3.7 Total Heat Requirement

The total heat requirement of the incubator (QT) is the summation of the heat energy required to raise the temperature of air (Qa) and egg (Qe) from 22^{0}C to 37.5°C; the heat loss through the wall of the structure (QS), egg tray and ventilation (QV).

$$Q_{T=Q_a+Q_s+Q_e+Q_v} \quad (3.28)$$

In determining the heat load of the egg incubator, the following assumptions were made:

- Incubator materials have a constant thermal conductivity
- The incubator is a closed system at a constant temperature.
- The required incubator temperature is 37.5^{0}C
- The room temperature is 22^{0}C
- The required humidity is 60%

i)Heat required raising the temperature of the air on the incubato**r:** measured air was flowing at the average velocity wind of 0.01m/s with density 1.22kg/m^3 and per unit area.

ma= 0.01m/s ×1.22kg/m^3 ×0.816m^2 = 0.04851kg/s

$Qa = m_a c_p (T_r - T_a)$ …………………………………...…… (3.29)

Qa = 155.5w

ii) Heat required raising the temperature of egg on the incubator: The average mass of one egg was weighed and found to be 60 g and the specific heat capacity of the egg was taken to be 3.18 KJ/Kg k

$$Qe = m_e c_{pe}(T_r - T_a) \quad \text{.......................................} \quad (3.30)$$

$$Qe = 3.08\text{KJ}$$

This is the total heat required to raise the temperature of the eggs from 22^{0}C to37.5^{0}C.

So, the total heat required for 50eggs = *3.08*KJ×50 = 154 KJ

This is the total heat required to raise the temperature of the eggs from 22^{0}Cto 37.5^{0}C. But this type of heat is provided gradually to prevent the eggs from boiling. Eggs transferred directly from the storage room to the incubator are heated at a rate of 0.30 ° C / min. whereas the pre-warmed eggs warmed at rates of 0.13°C and 0.16°C/min for the storage to room and room to incubator treatments, respectively. Now we considered our egg directly from storage with room temperature 22^{0}C the time required to raise this temperature to the incubator temperature is calculated.

$$t = \Delta T / warming\ rate$$

$$t = 51.66\text{min} = 3100\text{sec}$$

$$Q_e = Q_t\ e/\text{sec}$$

$$Q_e = 49.677\text{w}$$

3.7.1Heat loss of incubator

i) Heat loss on both sides of the incubator: The heat loss on both sides of the incubator can be calculated because they have the same surface area and are composed of the same material (plywood).

$$Q = \frac{A * K(\Delta T)}{L} \quad \text{.......................................} \quad (3.31)$$

Q_s = 0.952W but it was the opposite side

Q_s = 1.9W

ii)Heat loss at the top and bottom surfaces of the incubator: The top and bottom surfaces of the incubator were equal and opposite made of the same material. Area, A=0.262m^2

Since there were two equal surfaces,

$$A = 2 \times 0.262 m^2$$

$$A = 0.524 m^2$$

$$Q_{bt} = 1.9\text{W}$$

Heat Loss at the Front and Back of the Incubator

$$Q_{fb} = 1.9\text{w}$$

Therefore, the total heat loss: Q_{loss}= (1.9*1.9*1.9) =6.86w

iii)Heat required raising the temperature of egg tray (structure) on the incubator: There is an outer and inner box built from galvanized sheet metal of k=45W/mK^{-1}. In between the wooden boxes is an insulation material (fiberglass) of k=0.043W/mK^{-1}

QS was calculated using the equation:

$$Qs=\frac{As\Delta T}{\frac{Lwi+Lwo}{Kw}+\frac{Lins}{Kins}} \qquad (3.32)$$

Where, A_s=0.262m2

$L_{wi}=3*10^{-3}$m

$L_{wo}=3*10^{-3}$m

$L_{ins}=40*10^{-3}$m

$$Qs=\frac{0.262(37.5-22)}{\frac{0.003+0.003}{45}+\frac{0.04}{0.043}}$$

Qs=4.36w

There are four similar sides in the structure so total Qs=4.36*4=17.46 w

iv)Heat loss through ventilation (Qv)

Qv was calculated using equation

Where, V - ventilation rate =$ach \times volume\ of\ incubating\ unit/3600$

$$ach = air\ changes\ per\ hour$$

Therefore, the volume of the incubating unit (v) =0.149m^3

A suitable value of 2 air changes per hour was chosen.

Therefore, the ventilation rate =2 ×0.149m^3/3600 =0.827 ×$10^{-4} m^{3}/s$

$$\rho a\ at\ 37.5°C\ was\ found\ to\ be\ 1.135kg/m3$$

$$QV = \rho a \times V \times \Delta T = 1.135 \times 0.827 * 10^{-4} \times 15.5°C$$

$$QV = 0.00146W$$

$$\therefore QT = Qa + Qe + QS + QV$$

$$= 155.5 + 49.677 + 17.46 + 0.00146$$

$$QT = 222.6W$$

3.8Thermal Storage Capacity

Once the incubator is maintained with the required temperature the amount of heat supply is equal to the sum of heat loss through the incubator and ventilation loss

$$Qloss + Qv = 6.859 + 0.00148 = 6.86W$$

This is continuously supplied for 21 days. The total amount of energy stored on storage material = 6.86W ×use time 18hour×3600sec = 444.528KJ.

The amount of heat that can be stored by the ballast pebbles (Q_b) was calculated as shown below:

$$Qb = m_b C_{pb} [Tr - Ta] \qquad (3.33)$$

Where m_b - a mass of the ballast pebbles (kg)

C_{pb} - specific heat capacity of the ballast pebbles (J/kgK^{-1})

But m_b=0.75$\rho_b V_b$

Where ρ_b- density of the ballast pebbles (kg/m^3)

V_b - the volume occupied by the ballast pebbles (m^3)

0.75 = Void factor to correct for calculation of V_b Using the properties of ballast pebbles in table 1.2 in appendix 1

$$C_{pb} = \frac{680+880}{2} = 780\text{J/kg. K}^{-1}$$

$$\rho_b = \frac{2760+2770}{2} = 2765\text{kg/m}^3$$

The ambient temperature (T_i) was at 22˚C and the maximum temperature of ballast (T_b) is 50 ˚C.

$$\therefore Q_b = m_b \times 780 \times (50-22)\ ℃$$

$$m_b = 145.5\text{kg}$$

Volume needed = $mb/\rho b = 145.5kg/2765kgm3$ = 0.053m^3

The average sunshine hour of Bako in year month is 7.125 hrs = 7.125×3600sec = 25200sec.

$$= 444528kJ/25200sec.$$

$$= 17.64W$$

On an average lower sunny day, the sunshine hours are for 3.4 hours. Time =3.4 hours = 12240 seconds. Hence the rate of heat gained by the ballast pebbles is

$$Q_b = \frac{444.528kJ}{12240Sec} = 36.31\text{w}$$

3.9 COMSOL Simulation

COMSOL multi-physics software was a finite element analysis, solver, and simulation software program that could be used to address a variety of physics and engineering problems. COMSOL multiphysics simulation surroundings allow all steps for inside the modeling technique i.e. defining geometry, specifying physics, meshing, solving, after which post-processing the result [17]. In this research, a three-dimensional FE model was developed for the prediction of temperature distribution inside a solar collector at no-load conditions[18]. The fractional differential conditions on heat move were tackled utilizing a COSMOL Multiphysics® (Version 5.4). Warmth move in solids module with surface-to-surface radiation and outside radiation source highlight was utilized to represent heat move at no-load condition.

During solar incubation, air passes from the inlet vent to the flat plate collector followed by an incubator chamber to heat the egg inside the chamber, and finally exits through the outlet vent. Air is heated by convective heat transfer from the absorber plate and by receiving direct solar radiation. The solar-powered egg incubator condition was simulated with the following assumptions:

i. Air flows inside the solar incubator under steady-state condition
ii. There is no heat loss from the system

3.9.1 Model geometry

The geometry of the solar collector was created using COMSOL software based on the actual size of the system. It is consisting of an absorber plate, storage, and thermal insulation layers. Material properties were assigned to each part component. The solar irradiance is transmitted through the glass cover. Therefore, is incident on the absorber plate and converted into internal thermal energy. The ambient air at temperature T_{amb} is entering to the collector, it is streaming down the absorber plate and it gets heat from the absorber plate. The components geometry of the system is shown in the flowing figures with thermal and without storage layers.

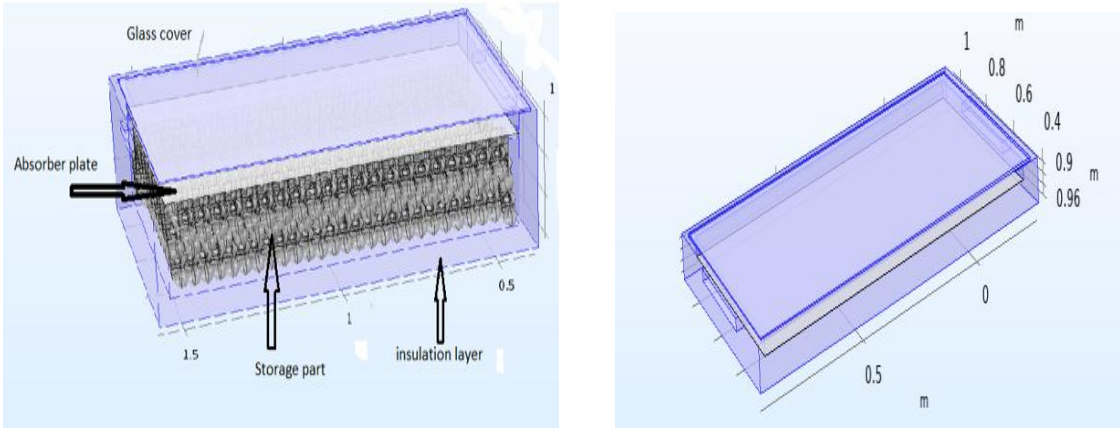

a) b)

Figure 3.6 Components of the FPSC model with(a) and without storage layers

The primary stage of the built FPSC model is the type of mesh. Therefore, many types of mesh have been created (see figure 3.8). The top boundary in the solar collector was assigned as glass and the rest of the boundaries were assigned to be aluminum. The shape and size of mesh elements influence the convergence and accuracy during FE analysis [19]. The extreme fine mesh structure was selected due to better convergence of the results. The completed meshed domain contained 667,929 tetrahedral, 124,908 triangular, 1,550 edge, 16 vertex elements, and average element quality 0.6591with storage layer and for without storage the completed meshed domain contained boundary elements: 1241688 tetrahedral, 10387 edge, 48 vertex elements, and average element quality 0.06334 with storage layer and for without storage

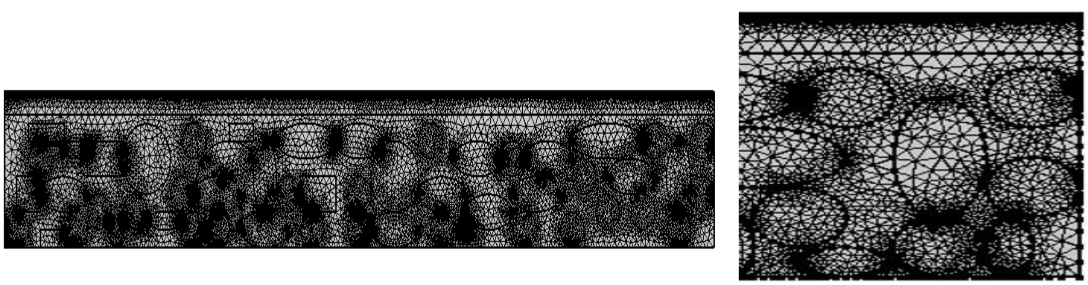

a)

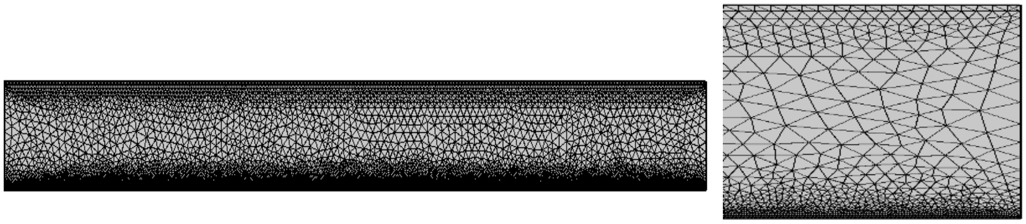

b)

3. **7** The mesh type for the FPSC model with storage(a) and without storage(b)

3.9.2 Governing equations

The mathematical model proposed to represent the transient heat transfer in a solar collector is given in the form of Fourier law of heat conduction.

$$\rho C_p \frac{\partial T}{\partial t} + q = Q \quad (3.34)$$

$$q = -k \nabla T \quad (3.35)$$

q = 0.7781w/m^2

Where ρ is the density (kg/m^3), C_p is the heat capacity (kJ/ kg K), T is the temperature (K), q is the convective heat flux (W/m^2), and k is the thermal conductivity of air (W/m. K). Since heat generation inside the incubator chamber is neglected, Q = 0, convective heat flux between absorber plate and the air is given as

$$-n \, . \, q = q_o \quad (3.36)$$

$$q = h_{c,p-a} \left(T_p - T_a\right) \quad (3.37)$$

q = 203.36 w/m^2

Heat transfer in the diffuse surface is presented as:

$$-n . q = \varepsilon(I - e_b(T)) \quad (3.38)$$

$$(1 - \varepsilon)I = J - \varepsilon eb(T) \quad (3.39)$$

$$e_b((T) = n^2 \sigma T^4 \quad (3.40)$$

q=661.37w/m^2

Were q_0 is the inward heat flux, $h_{c,p-a}$ is heat transfer coefficient between plate and air and, I am the total incoming radiative heat flux (W/ m^2), $e_b(T)$ is the blackbody emissive power (W/m^2), ε is the emissivity of glass, J is the total outgoing radiative flux (W/m^2), and σ is the Stefan-Boltzmann constant (W/m^{2}K^4).

3.9.3 Boundary conditions

Initially, the temperature of the air was considered to be uniform throughout the system

$$T_a = T_0$$

$$at\ t = t_o \ldots\ldots\ldots\ldots\ldots\ldots\ldots\ldots\ldots\ldots\ldots\ldots \quad (3.41)$$

$$T_a = 22^0\text{C}$$

The boundary condition for a solar collector is given in the table

Table 3. 3 Boundary conditions used for FE modeling of solar incubator

Solar collector	*Boundary condition*	*Governing equation*
1(Glass)	Diffusive surface	$q = \varepsilon(I - e_b(T))$
6 (absorber plate)	Convective heat flux	$q = h_{c,p-a}(T_p - T_a)$
2, 3,4,5 (wall)	insulation	$-n \cdot q = o$

3.8.4 Simulation Parameters

Material properties data for aluminum and glass were provided by COMSOL Material Browser as shown below in Table.

Table 3. 4 List of material properties used in the model

	Units	*Aluminum*	*Glass*
C_p	J/Kg. K	900	703
ρ	Kg/m3	2710	2203
k	W/m. K	239	1.38
E	Pa	70E9	73.1E9
β	1/K	2.3E-5	0.55E-6

Where E is Young’s modulus and β is the coefficient of thermal expansion

3.10 Construction of the System

The prototype of the solar-powered egg incubator with a sensible thermal energy storage system was constructed at the workshop of Bako Agricultural Engineering research center of Oromia Agriculture research institute. All Materials used to fabricate were selected based on local availability and cost-effectiveness.

Table 3. 5 Parts components of solar-powered egg incubator materials list

s/no	Part components	Part Description	Dimensions (cm)	Quantity
1	Glazing glass	Used to collect solar radiation and prevent entrance of debris	120×72×0.35	01
2	Absorber	aluminum sheet metal painted with thick black	114×62×0.9	01
3	Chamber (Front wall) Chamber (side walls) Camber (bottom)	Made of ply wood	57×50 50×57 57×50	01 02 01
4	Chimney (front and back) Chimney (side walls)	Made of wood structures and galvanized sheet	0.2×0.3 0.3×0.4	02 02
5	Egg tray	Made of wood and mesh wire	45*40*0.4	02
6	Pan	Made of mild steel	0.2*0.5	01
7	Locks	To secure the window closing without permission	Standard	03
8	Hygrometers	To measure humidity	Standard	02
9	Ballast pebble	Store energy	m^3	02
10	Thermo stat	To control temperature	STC 1000	01
11	Thermometers	To measure temperature	Standard	02
12	Infrared thermo meters	To measure beam radiation	standard	01

3.10.1 Fabrication process

a) Cutting, molding, and component fabrication

The fabrication of the incubator chamber has been performed using plywood, galvanized, mesh wire, and fiberglass. Those materials were used because they are cheap. They have an excellent machinability character and good thermal properties. Those materials were cut according to the design dimensions using a wood circular saw, wood planning machine, scissors, and parts that need molding process is performed using adhesive chemicals and nails as shown in the figure below.

Figure 3. 3 constructed incubator chamber

b. Assembling

Different parts of the solar-powered egg incubator like incubator chamber, chimney, and absorber plate, built-in thermal energy storage, sidewalls, and trays are assembled with permanent fasteners (nails). The glass and the fan inlet are cut as per the design and assembled as shown below.

Figure 3. 4 Solar collectors with energy storage construction assembling

c) Finishing

Finally, the absorber plate and essential parts of the solar-powered egg incubator were painted thick black to minimize radiation heat losses and increase the performance of the absorber.

Figure 3. 5 Final views of the solar incubator

3.9.2 Equipment and Instruments

The following measuring instruments have been used as shown in the table below

Table 3. 6 Measuring instruments

S/no	*Equipment*	*Function*
1	Infrared thermometer	To measure solar radiation on a black flat plate
2	k-type thermocouple	To measure chamber, collector, and glass temperature
3	Thermo hygrometer	To measure ambient air and air relative humidity
4	Digital multi-meter	To measure the temperature inside of collector in (mv)
5	thermometer	To measure ambient temperatures
6	Thermostat	To control the temperature the chamber

Figure 3. 6 Humidity and ambient temperature measuring devices

Figure 3. 7 Temperature measuring instruments

Figure 3. 8 Temperature controller device (Thermostat STC 1000)

3.11 Experimental study

After system manufacturing, and assembling were completed, the performance of the solar collector and solar-powered egg incubator was carried out in Bako engineering Agricultural research center which includes the physical and biological tests.

3.11.1 Test of systems before loading

The physical tests were conducted on the constructed solar-powered egg incubator, with the thermal energy storage system. Its aspects involve monitoring the temperature and the relative humidity of the incubator as well as that of the ambient to determine the suitability of the system to hatch poultry eggs[20]. This was done for 24 hours and some modifications were done on the solar-powered system before loading the eggs to avoid intermediate failure during the incubation period.

3.11.2 Test After Loading

A total of 25 eggs were purchased while 20 eggs were successfully loaded for the performance evaluation of the egg incubator. 2 eggs out of the 20 eggs loaded were broken during the Candler test on the 5th day was conducted. But Proper tracking changed into carried out at the solar-powered system and the egg incubator because of the sensitivity inside the process of hatching of the eggs. More so, the inner temperature of the incubator was monitored using a temperature controller (thermostat STC 1000 China model), and relative humidity was measured using the digital thermo hygro-thermo meter. Temperatures of different components of the solar collector and solar radiation were measured during 21 days of incubation. Those days data were taken to study the effects of the solar collector temperature on the incubator chamber without any active supplementary heating system attached to it. The measurement data have taken for 10 hours, beginning from 8:00 to 17:00 in the 1 hours' time intervals. The hourly temperature measurements were done by using k-type thermocouples fixed at the absorber plate used to measure the temperature of the collector (Tp), at storage (Ts), and other k type thermo-couple were attached at the outlet of the solar collector to measure hot air at collector outlet (To). These temperature values are read from the table at the millivolts of the thermocouple. While the hourly solar radiation was measured for 21 days of the incubation period.

Figure 3. 9 Solar powered egg incubator controller device adjustment and reading

The World Meteorological Organization (WMO) and the International Standards Organization (ISO) define scientific standard types of instruments. In a solar monitoring station, solar radiation is measured in three ways, they are:

i. Horizontal flat plate for the beam solar radiation measurement
ii. Pyrheliometer used to measure direct beam radiation
iii. Pyranometer used to measure total radiation

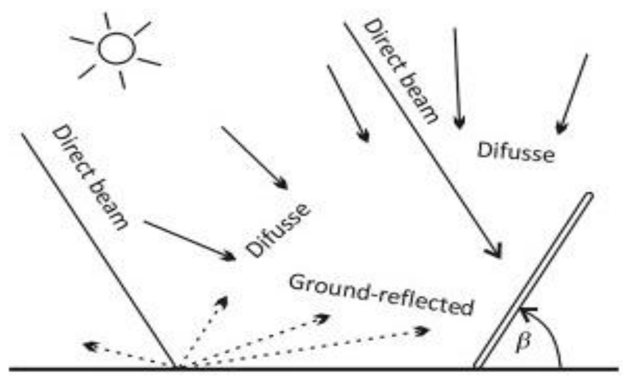

Figure 3.10 World measurement organization solar radiation quantities[15]

to measure beam radiation, the black-coated horizontal flat plate is used. The one plate is placed directly to solar irradiance. Then measure the temperature of the black surface for both plates within the time intervals by an infrared thermometer without touching.

Figure 3. 11 Setups of the instrument used for temperature measurement

The temperature of the plate placed directly to the solar irradiance is replaced by T_s and T_a is the atmospheric temperature recorded within the same time and time intervals by using the thermometer. The time interval between any two readers is1hour. All the measurements value was tabulated in appendix B table B.1 and B.2. The solar radiation is calculated from the energy balance equation on the black-coated surface.

$$I * A_S * \alpha = h * A_S * (T_s - Ta) + \varepsilon * \sigma * As * ({T_s}^4 - {T_{sky}}^4) \ldots\ldots\ldots\ldots (3.28)$$

During this experiment, the loaded eggs were turned five times daily at intervals of 3 hours to avoid egg yolk from sticking on the shell. However, the turning of the eggs was stopped after day 18 to allow the embryos time to start piping [21].

Candling is a technique used to notice the development and advancement of an incipient organism inside an egg which utilizes a brilliant light source behind the egg to show subtleties through the shell[18]. It is purported that the first wellsprings of light utilized were candles [21]. A Candler was utilized to decide the rate richness of the eggs on the fifth day,14th day, and on the seventeenth day wherein break, fruitless, and dead undeveloped organisms were recognized[21][22].

The percentage fertility and hatchability were obtained from the equations below respectively.

$$\% \text{ Fertility } = \frac{\text{Number of fertile eggs}}{\text{Number of eggs loaded}} * 100\% \ldots\ldots\ldots\ldots\ldots\ldots\ldots\ldots \quad (3.29)$$

$$\% \text{ Hatchability } = \frac{Number\ of\ egg\ hatched}{Number\ of\ fertile\ eggs} * 100\% \ldots\ldots\ldots\ldots\ldots\ldots \quad (3.30)$$

CHAPTER FOUR

4. RESULT AND DISCUSSION

4.1 Solar Energy Potential of the Study Area

In this section, the results of the simulation, experimental work, and available solar potential of the study area were presented. In addition, the performance analysis of the flat plate solar collector was discussed. To estimate available solar energy resources of the area, the relevant data was collected from the National Meteorological Agency of Bako agricultural research center (NMA) during the sunshine hours. The solar potential calculated results for data collected from the NMAS are tabulated in the below table.

Table 4. 1 Solar radiation calculated from meteorology data at the sunshine hour of Bako

Months	*n*	n_s (*hr*)	*dec*	ωs (°)	N_s (*hrs*)	*a*	*b*	*H* (MJ/m^2)	H_d (MJ/m^2)	H_b (MJ/m^2)	H_o (MJ/m^2)
January	17	8.5	-20.92	86.53	11.54	0.33	0.40	20.80	6.98	13.82	33.4
February	47	8.6	-12.95	87.91	11.72	0.32	0.40	21.04	7.02	14.02	34.3
March	75	7.9	-2.42	89.61	11.95	0.30	0.43	21.56	8.47	13.09	36.9
April	105	7.4	9.41	91.5	12.20	0.28	0.46	20.91	9.14	11.77	37.4
May	135	7.1	18.79	93.1	12.41	0.28	0.45	21.87	10.18	11.69	40.7
June	162	5.8	23.09	93.87	12.52	0.24	0.50	18.77	10.40	8.38	39.8
July	198	3.6	21.18	93.51	12.47	0.19	0.56	14.74	10.26	4.48	41.9
August	228	3.4	13.45	92.16	12.29	0.18	0.57	13.41	9.46	3.94	39.7
September	258	4.7	2.22	90.35	12.05	0.22	0.53	15.49	9.50	5.99	36.3
October	288	7.5	-9.60	88.47	11.80	0.29	0.44	20.45	8.46	12.00	35.9
November	318	8.7	-18.91	86.89	11.59	0.32	0.40	21.84	6.98	14.86	35.2
December	344	8.9	-23.05	86.14	11.49	0.33	0.39	22.00	6.61	15.40	34.8

The following graph is showing the monthly average global radiation, diffuse radiation, and beam radiation for the National Meteorological Agency of the study area. The results were obtained from solar radiation calculations, by using meteorology data and sunshine hours of the locations 9.06 altitudes and 37.09 longitudes.

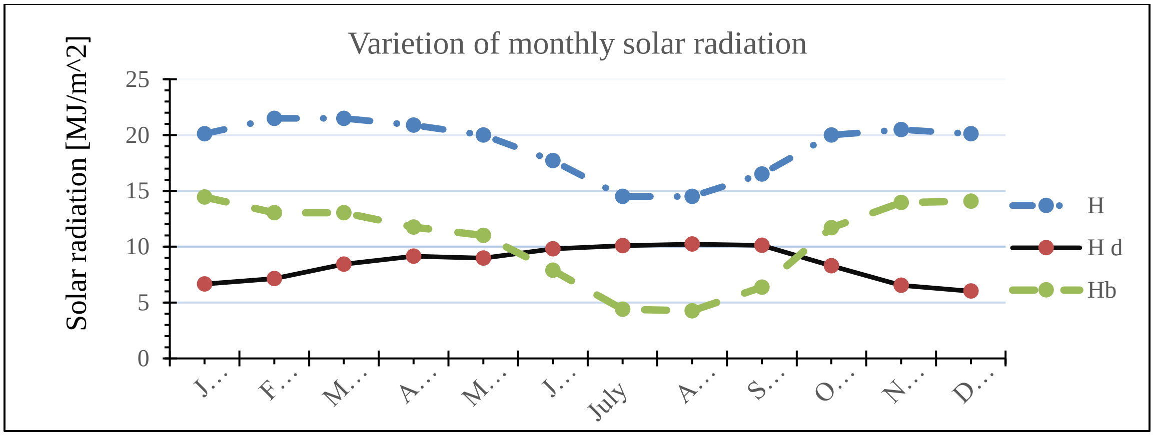

Figure 4. 1 Monthly average Global, Diffuse and Beam solar radiation of NMSA BACR

The Variation of solar radiation of each day gives the different energy potential in the year. According to this National Meteorology Agency data, the peak value of the beam radiation for Bako is 14.02 MJ/m^2 in February. In addition, the minimum beam radiation is 3.94MJ/m^2 occurs in July and the annual average beam solar radiation is 10.79 MJ/m^2. The comparison of the available solar energy resource data collected from three of the meteorological stations NASA Surface meteorology, (NMA), and the SWERA website is discussed in the below table.

Table 4. 2 Monthly average daily solar radiation of study the area from three meteorology station

Months	***NMSA (kWh/m^2/day)***	***NA (kWh/m^2/day)***	***SWERA (kWh/m^2/day)***	***Sunshine hours***
January	5.78	6.34	5.9	8.5
February	5.84	6.29	6.01	8.6
March	5.99	6.4	5.45	7.9
April	5.81	6.37	5.73	7.4
May	6.08	6.12	5.32	7.1
June	5.21	5.42	4.80	5.8
July	4.09	4.42	4.01	3.6
August	3.73	4.45	4.23	3.4
September	4.30	4.83	4.63	4.7
October	5.68	6.19	6.12	7.5
November	6.07	5.20	5.60	8.7
December	6.11	5.72	5.72	8.9

The variation of direct solar radiation observed from different meteorology station

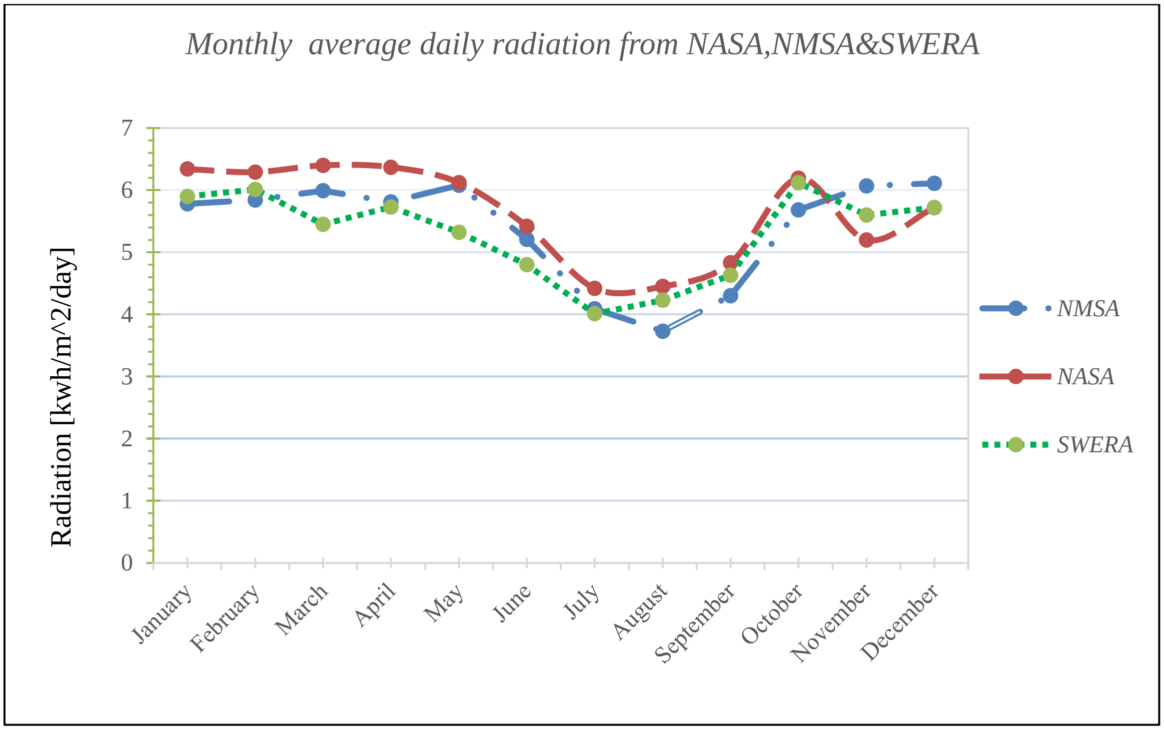

Figure 4. 2 Monthly Average Daily Solar Radiations from NMSA, NASA& SWERA

The monthly average daily solar radiations from these different meteorological stations for the study area are 5.65 kWh/m^2 for NASA, 5.29kWh/m^2 for the SWERA Database website, and 5.39 kWh/m^2 for NMA. The above results are the monthly average solar radiation in the study area observed from different meteorology stations and the monthly average daily solar radiation of NMSA is close to SWERA than NASA. The variation of solar radiation results depends on the time of day, Geographical features, and the season. From the hypothesis, the atmospheric conditions can reduce direct radiation by 10% on clear, dry days and by 100% on thick, cloudy days.

The literature that compared with the present results was done at North East Jimma town Serbo woreda at 7.44^{O}N and 1844m elevation by [23]. The result shows the total solar radiation of Bako is better than Serbo with average total radiation of 5.39 kWh/m^2/day for the present study area Bako Tibe woreda and 5.13 kW/m^2/day for Serbo Woreda (from literature).

In the present, study the flat plate solar collector receives the beam radiation to the absorber plate and transmitted energy to the storage system, the incoming solar radiation (insolation) directly measured during experimental work. To this end, the horizontal flat plate setup was conceived to be capable of measuring the direct solar radiation of the study area.

Experimental results on solar beam measurements

The experiment was conducted for 21 days under normal weather conditions of the study area in may (05, 10, and 15, 2021) for eleven hours per day. The selection of days was based on the intensity of solar radiation estimated before experiments (i.e highest, lowest radiation, and monthly average daily solar radiation). The measured data for three days was listed in appendix B table B.1. the following figure shows the variation of beam obtained from measured temperature by the black painted plate at the same time interval in three days.

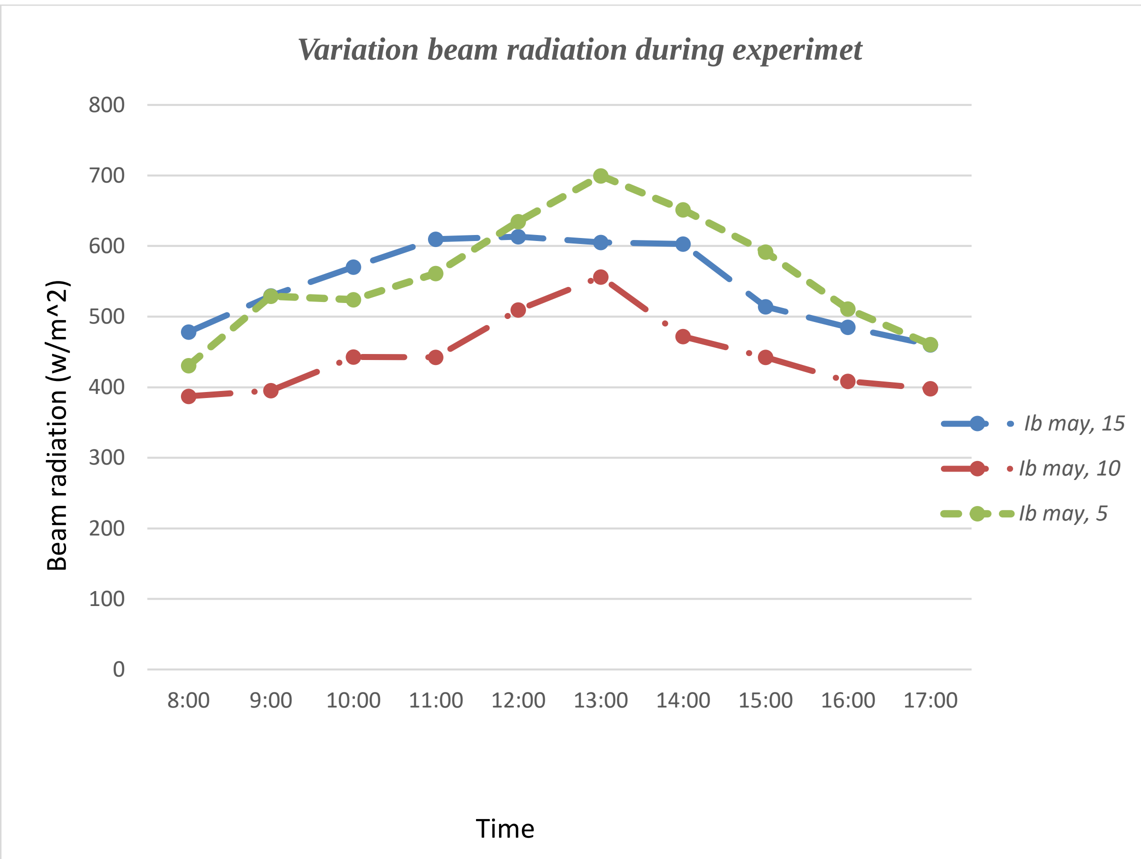

Figure 4. 3 Variation of solar radiation calculated results from measured temperatures by the black painted horizontal plate.

The maximum values of the beam solar radiation observed during the experiment are 669.7 W/m^2 at 13:00 May 05,2021 and the minimum values of beam radiation obtained May 10.2021 at 8:00 am. The results of solar thermal energy depend on the intensity of solar radiation, and the solar radiation may be affected by the weather condition such as the presence of clouds and the angles of sun forms to the earth. During the experimental studies, the weather condition of the study area for the first day of May 05 is a clear sky, sunny and no cloud was seen. For this purpose, relatively higher solar radiation was observed on this day. However, on May 15 sunny, but the small scattered cloud has seen about 9:00 am to 11:00 am. Additionally, on May 10, the Bako weather condition is a clear sky and sunny before and afternoon. However, the passing cloud was seen around solar noon. Figure 4.4 shows the comparison of average experimental solar beam radiation results with average estimated.

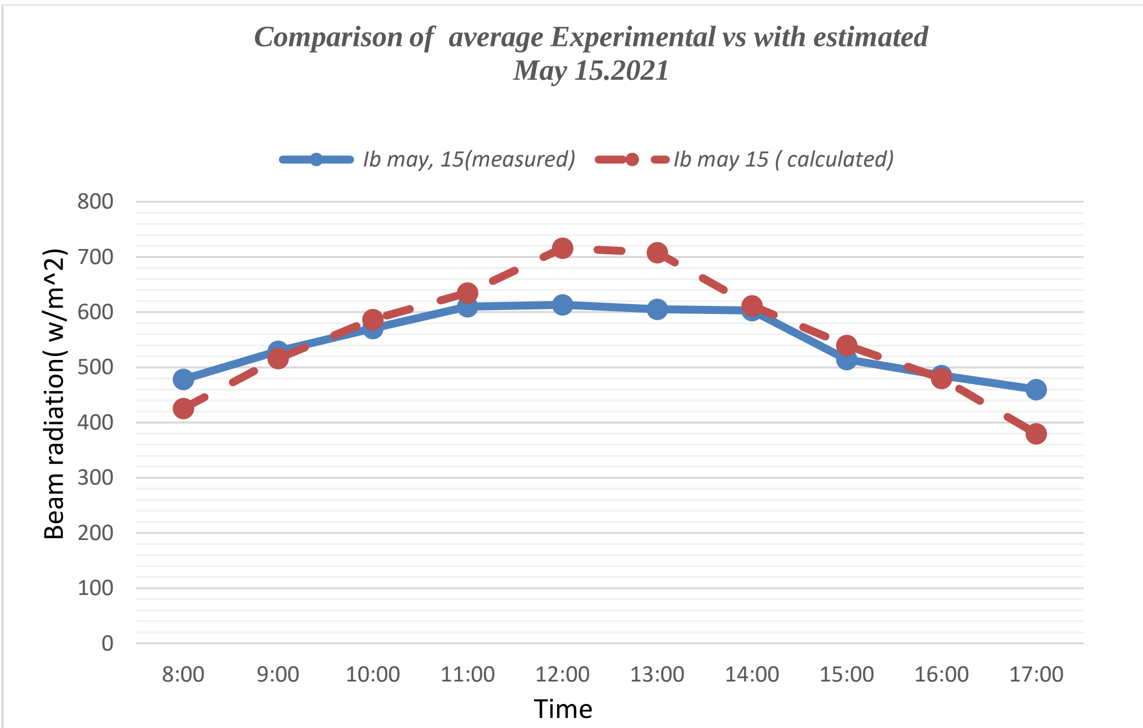

Figure 4. 4 The comparison of experimental data with calculated

A significantly similar solar radiation results between the experimental data and calculated. However, the experiment is conducted for a few days and it may be difficult to decide the monthly data by three-date data. The maximum average beam radiation observed from experimental and calculate are 613.3W/m^2 and 716 W/m^2 at 13:00 respectively

4.2 Simulation Result

4.2.1Temperature distribution profile of air

The temperature distribution profile inside the solar collector at the normal condition for every 2 hr interval of time is depicted in Figures 4.5; the absorber plate temperature range varies in each figure. At time t = 0, the temperature inside the solar collector was almost uniform as shown in the table below.

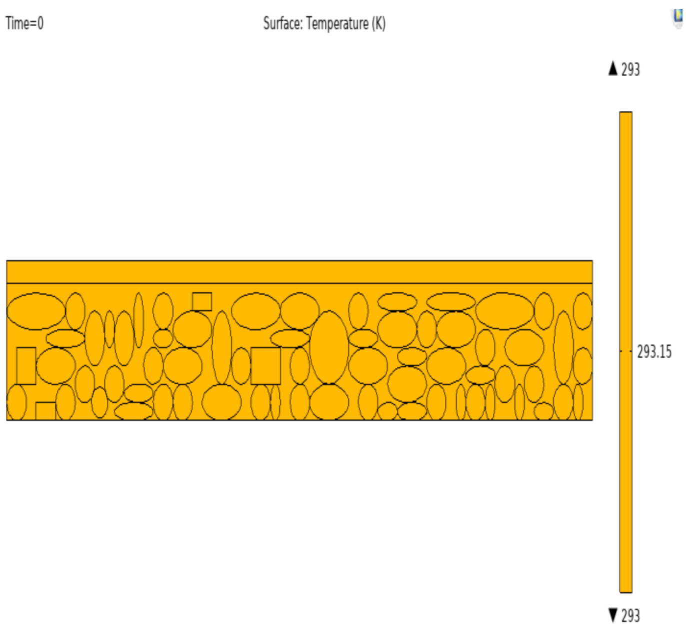

x	y	Value
0.31174	0.020823	293.15
0.39131	0.010388	293.15
0.38739	0.039084	293.15
0.37826	0.070388	293.15
0.37826	0.070388	293.15
0.36913	0.16169	293.15
0.36913	0.12778	293.15

As time proceeded, the temperature of air adjacent to the absorber plate increased as visualized from the figures. The black enamel coating in the absorber plate has an absorptivity value of 0.90 and thus it absorbs most of the radiation incident on it. The temperature of the glass cover is less due to its low absorbance, thus air temperature at the top is low as can be inferred from the figures. The air is heated by heat transfer due to convection from the absorber plate and direct radiation from the sun. It can be also noted that the temperatures at various locations of the collector were different at any given time.

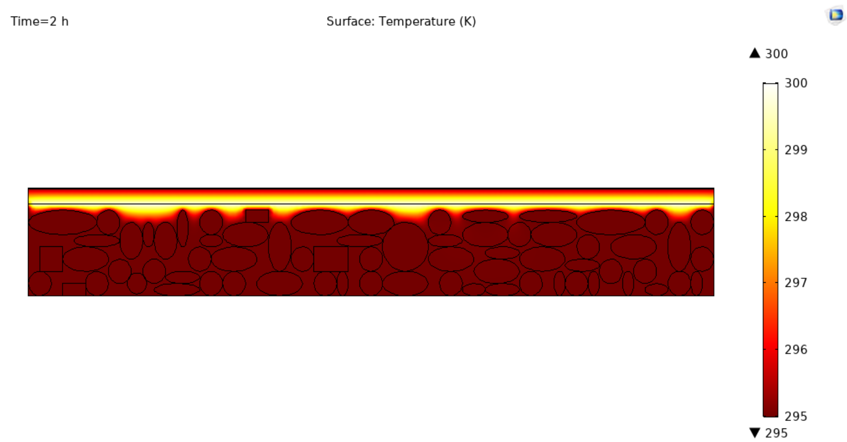

x	y	Value
1.1452	0.14676	299.38
1.1452	0.15496	299.05
1.1452	0.16725	296.68
1.1452	0.17272	295.63
1.1794	0.16452	297.19
1.1766	0.16725	296.67

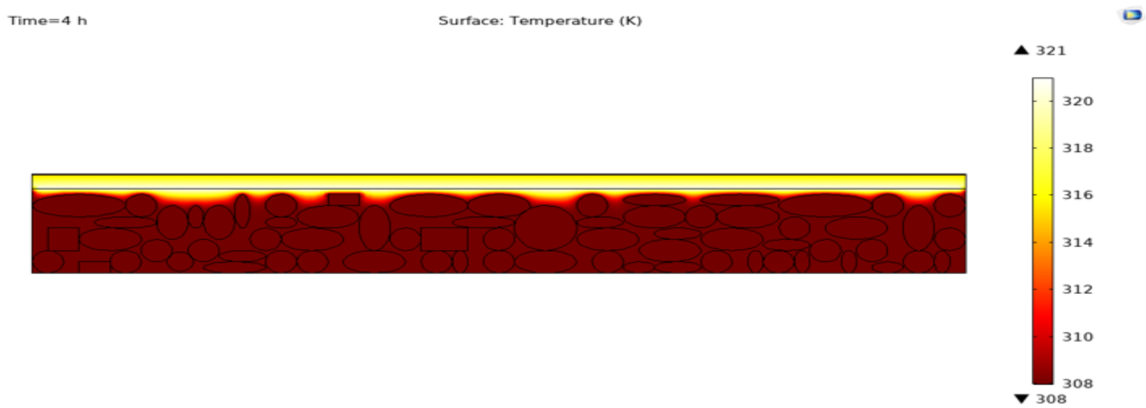

As can be seen, in the solar collector, the temperature gradient at the inlet side and outlet side of the system remains consistent. The temperature of the air stayed constant throughout the collector's length system remains consistent.

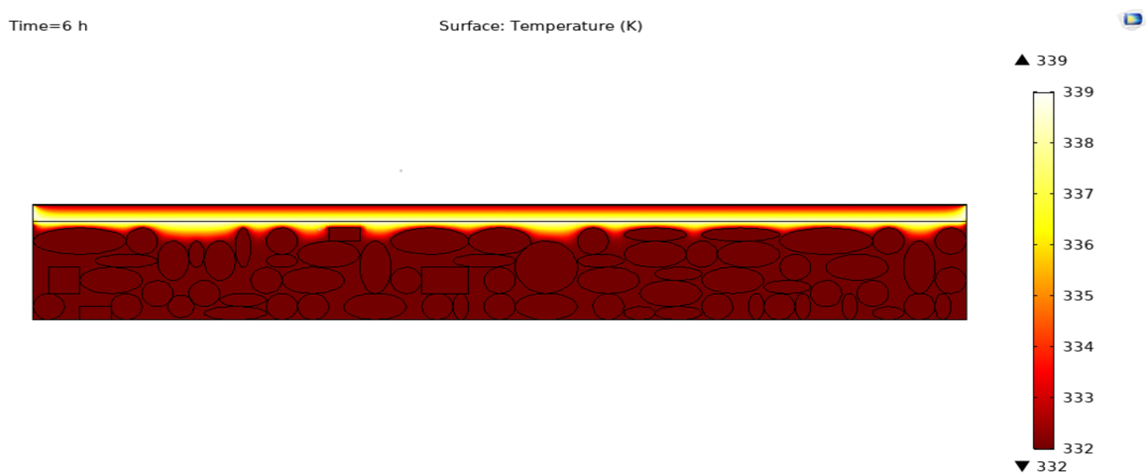

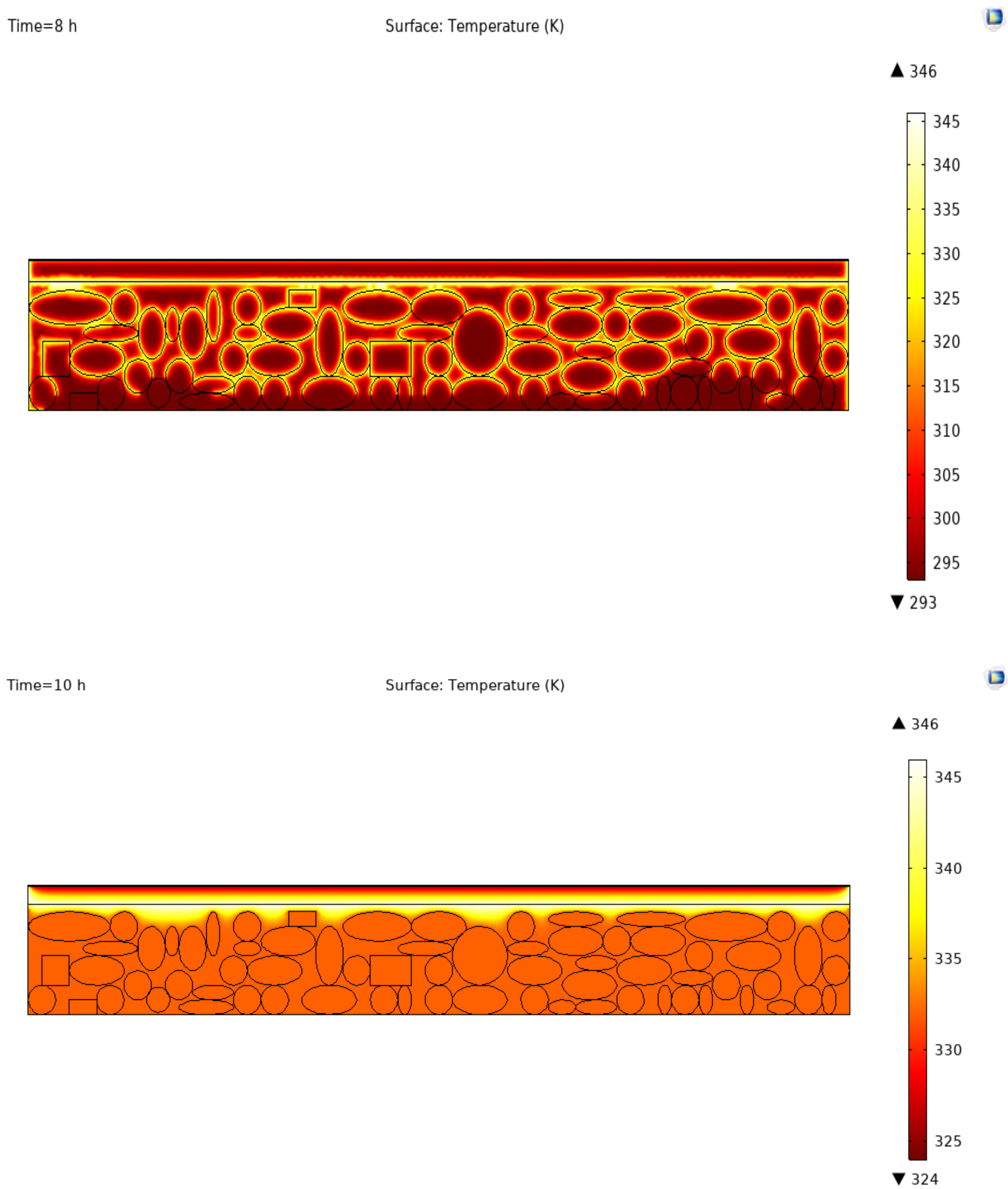

Figure 4. 5 Temperature distribution profile for the collector with storage along with the flow

The above figures show that the temperature distribution in the FPSC monthly average day for ten hours. The maximum temperature obtained 346k at 8:00(local time) in the absorber plate.

The typical variation of different temperatures of solar collector air heater with no energy storage at the different hour interval was simulated, as shown in the figures.

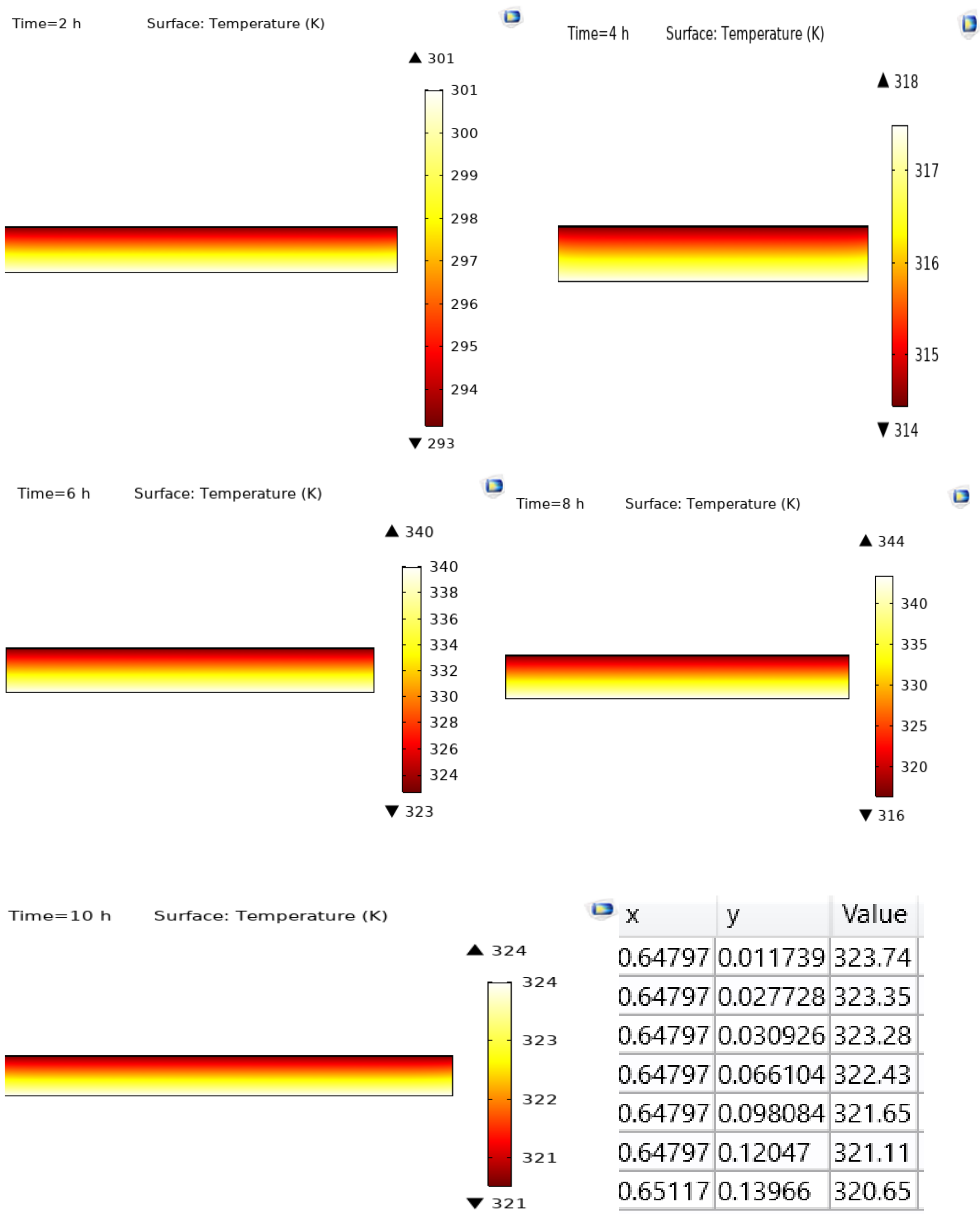

x	y	Value
0.64797	0.011739	323.74
0.64797	0.027728	323.35
0.64797	0.030926	323.28
0.64797	0.066104	322.43
0.64797	0.098084	321.65
0.64797	0.12047	321.11
0.65117	0.13966	320.65

Figure 4. 6 Temperature distribution profile for collector without storage along with the flow

The above figures depicted that the temperature distribution in the FPSC one day for Ten hours. The maximum temperature was 340k, in the absorber plate at 6:00 local time. It starts with the gradual escalation with the solar radiation increase. When there is no energy storing material, the maximum temperature reached by air is comparatively less and during the evening there was a high fall rate in the temperature.

4.3 Experimental Results after loading egg into the incubator

During the experiment, various parameters were recorded in a variety of days starting from May 1 up to 22, 2021. Among those days' typical data were taken for analysis for three days only (05, 11, and 15 May). The selection of days was based on the intensity of solar radiation (i.e highest, lowest radiation, and monthly average daily solar radiation). All the measured data was listed in tables.

Table 4. 3 Experimental measurements data on May 05, 2021

Time interval (hrs)	$T_a(^0C)$	$T_s(^0C)$	$I(w/m^2)$	T_p (mv)	$T_p(^0C)$	T_g(mv)	$T_g(^OC)$	T_o(°C)
8:00	20	30	430.6	1.68	41.69	1.43	35.55	38
9:00	19.5	36	529	2.012	49.76	1.64	40.7	47
10:00	21.5	43.5	570.1	2.12	52.38	1.67	41.45	48.4
11:00	23	42.2	561.2	2.43	59.86	1.72	42.67	49.3
12:00	24.5	45.5	634.5	3	73.5	2	49.47	55
13:00	25.6	60.1	699.7	2.75	67.56	1.75	43.4	51
14:00	27	63.1	651.5	2.023	50	1.68	41.69	48.6
15:00	26	55.3	591.6	2.26	55.76	1.93	47.7	45.2
16:00	25	43.2	511	2.55	62.99	1.92	47.53	46.2
17:00	24	35	460.7	2.01	49.71	1.63	40.47	43.7
18:00	23.1			1.96	48.5	1.5	37.29	40.1
19:00	23							39.4
20:00	23.7							39.1
21:00	22.1							38.6
22:00	22							38
23:00	21.7							37.2
24:00	21							36.1

Table 4. 4 Experimental measurements data on May 10, 2021

Time (hrs)	$T_a(^0)$	$T_s(^0)$	*I(w/m)*	$T_p(mv)$	$T_p(^0)$	$T_g(mv)$	$T_g(^O)$	$T_o(°C)$
8:00	16	22	387.2	0.89	22	0.86	21.5	22
9:00	19.5	23.5	395.1	1.1	27.45	0.9	22.5	25.1
10:00	21.5	32.1	443	1.16	28.93	1.47	25.7	27
11:00	23	32	442.4	1.76	43.64	1.52	34.84	36.2
12:00	25	43	509.7	2.26	55.76	1.78	44.13	48
13:00	25.6	50	556.4	1.68	41	1.59	39.49	40.1
14:00	22	37	472	2.023	50	1.68	41.69	46
15:00	22.3	32	442.4	2.26	55.76	1.73	42.9	43.8
16:00	22	26	408.6	1.53	38.03	1.39	34.5	35
17:00	22.1	24	397.8	1.47	36.5	1.35	33.6	34
18:00	19			1.93	35.2	1.06	31.5	33.3
19:00	18.5							32.8
20:00	17.2							32.1
21:00	17							31.5
22:00	17.3							30.7
23:00	16.4							29.6
24:00	15.1							29.4

Table 4. 5 Experimental measurements data on May 15, 2021

Time interval (hrs)	$T_a(^0C)$	$T_s(^0C)$	$I(w/m^2)$	T_p *(mv)*	$T_p(^0C)$	$T_g(mv)$	$T_g(^OC)$	$T_o(°C)$
8:00	18	38	478.2	1.123	28.03	1.62	31.78	28
9:00	19.5	46	529.3	1.31	32.72	1.64	40.7	32.1
10:00	21.5	52.5	570.3	1.71	42.38	1.67	41.45	41
11:00	23	57.2	609.9	2.22	54.86	1.72	42.67	46.3
12:00	25	58.5	613.3	2.3	58.68	2	49.47	56
13:00	25.6	60.1	629.3	2.43	59.93	1.75	43.4	55
14:00	27	63.1	603.1	2.44	60.1	1.68	41.69	48.6
15:00	26	55.3	514.2	2.31	56.76	1.73	42.9	50.2
16:00	25	50.6	485.1	2.32	56.99	1.92	47.53	47.3
17:00	24	35	460	2.25	55.71	1.63	40.47	42
18:00	23.1			2.17	53.64	1.52	37.08	39.1
19:00	21							38.4
20:00	20.4							38
21:00	20							38.2
22:00	20.1							37.8
23:00	18.3							36
24:00	16							35.3

The performance of the flat plate solar collector was evaluated by measuring the solar radiation, temperatures of the glass cover, absorber plate temperatures, inlet (ambient air), and outlet air of the collector during the experimentation.

a) **Results of measured collector outlet, ambient air temperatures, and a typical day of highest solar radiation (May 05, 2021).**

The variations of ambient temperature, collector outlet temperature, and solar radiation intensity for typical days of highest solar radiation, during 21 days of incubation are shown in Figure 4.4. The maximum collector outlet temperature and maximum ambient air temperature obtained for the day of highest solar radiation were 55^{0}C and 27^{0}C during daylight at 12:00 am and 14:00 respectively, while the minimum values obtained for lowest solar radiation were 38^{o}C and 20^{0}C during daylight respectively. During the test, a maximum collector thermal efficiency of 44.33% was obtained. The high temperature obtained in the solar collector helps maintain the design temperature of 37.5^{0}C in the incubating chamber with slight fluctuations between+2^{0}C and –2 ^{0}C throughout the incubating period.

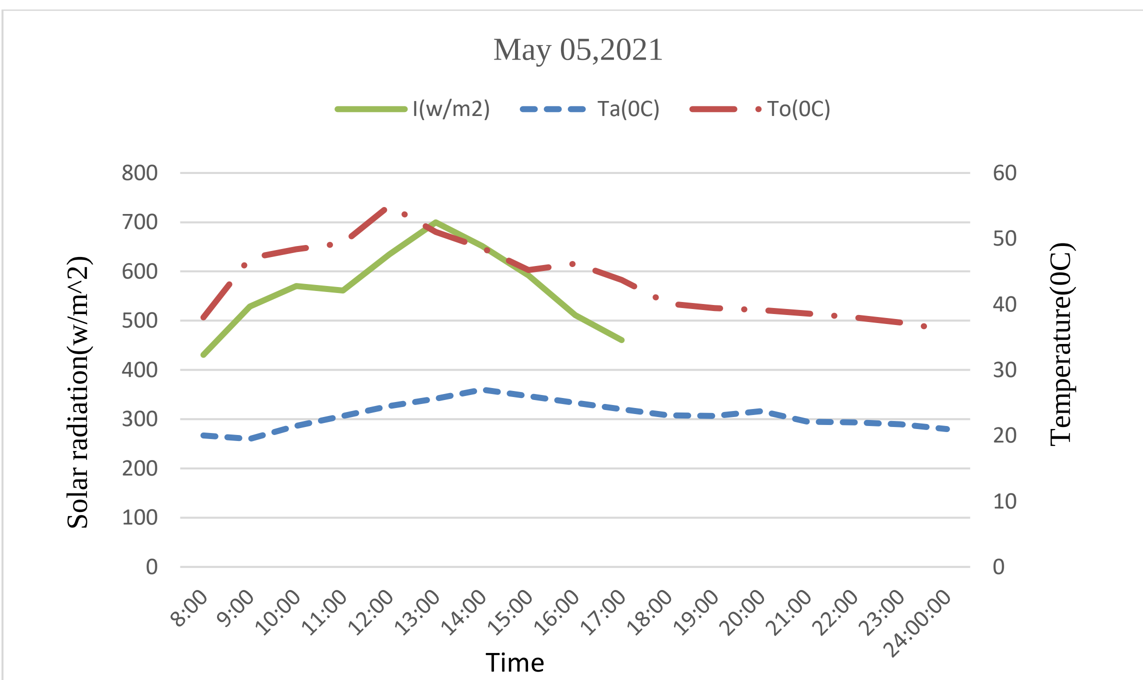

Figure 4. 6 Variation collector outlet, ambient air temperatures, and solar radiation

b) Results of measured outlet air, ambient air temperatures, and lowest solar radiation day (May 10, 2021)

The variations of ambient temperature, collector outlet temperature, and solar radiation intensity for typical days of lowest solar radiations during 21 days of incubation are shown in Figure 4.5. The maximum collector outlet temperature and maximum ambient air temperature obtained for the day of lowest solar radiation were 48^{0}C and 25.5^{0}C during daylight at 12:00 am and 13:00 respectively, while the minimum values obtained for lowest solar radiation were 22°C and 15.1^{0}C during daylight at 18:00 and 24:00 respectively. During the test, a maximum collector thermal efficiency of 23.2% was obtained.

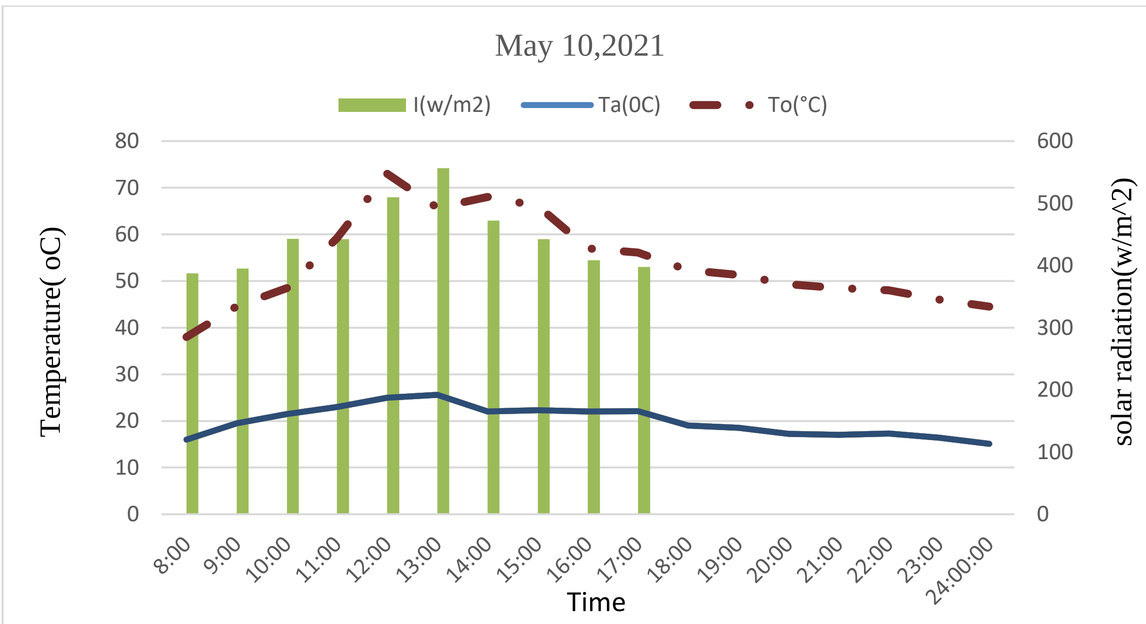

Figure 4. 7 Variation collector outlet, ambient air temperatures, and lowest solar radiation

The variation of the average temperature of the glass cover, absorber plate, and ambient air of experimental results for a test period from 8.00 AM to 17.00 is shown in Figure 4.6. It can be observed that the variation of absorber plate temperature was dependent upon the solar radiation intensity, increased in the morning, reaching a peak in the noon, and gradually decreased in the afternoon. The maximum outlet air temperature was recorded to be 55°C at noon. The solar radiation intensity varied between 460–699.5 W/m^2 during experimentation.

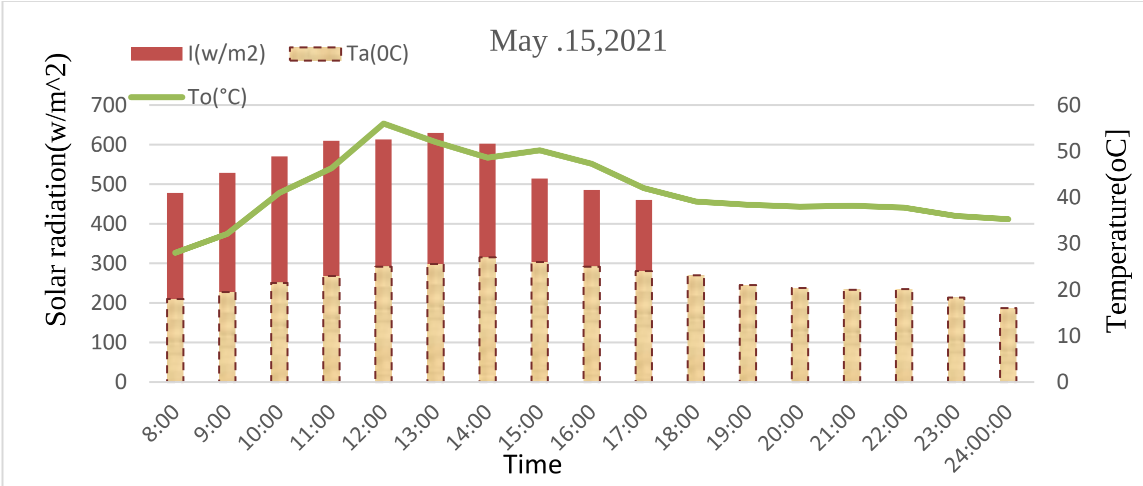

Figure 4. 8Average of air outlet temperature, and ambient against solar radiation

4.3.1Thermal efficiency of solar collector

As the solar intensity of the study area increases, more useful energy is captured. As the energy captured to increase the plate temperature raises and heat captured by the plate is partially transmitted to the storage compartments that were increased the temperature of the thermal storage systems. Hence, the system thermal efficiency results at the different values of solar beam radiation are tabulated in the below table.

Table 4-6 System thermal calculation for average solar radiation of May 15,2021

Time	*Q_g(w) storage*	*Q_g(w)without storage*	*I_t (w/m^2/h)*	*Efficiency with storage, η (%)*	*Efficiency without storage, η (%)*
8:00	10	9.67	478.2	0.03	0.03
9:00	37	27.39	529.3	0.11	0.08
10:00	108	93.80	570.3	0.30	0.26
11:00	119	112.38	609.9	0.33	0.31
12:00	149	152.26	613.3	0.36	0.37
13:00	200	194.4	629.3	0.44	0.43
14:00	148	128.90	603.1	0.38	0.33
15:00	118	92.44	514.2	0.33	0.26
16:00	99	65.46	485.1	0.30	0.20
17:00	96	45	460	0.29	0.14

The thermal efficiency of the system is the ratio of useful heat to the total heat received by the collector area. The corresponding thermal efficiency is directly proportional to useful heat. System thermal calculation results for the experimental measurements of average solar radiation in the time intervals to calculate the efficiency of the solar collector were discussed in the following tables.

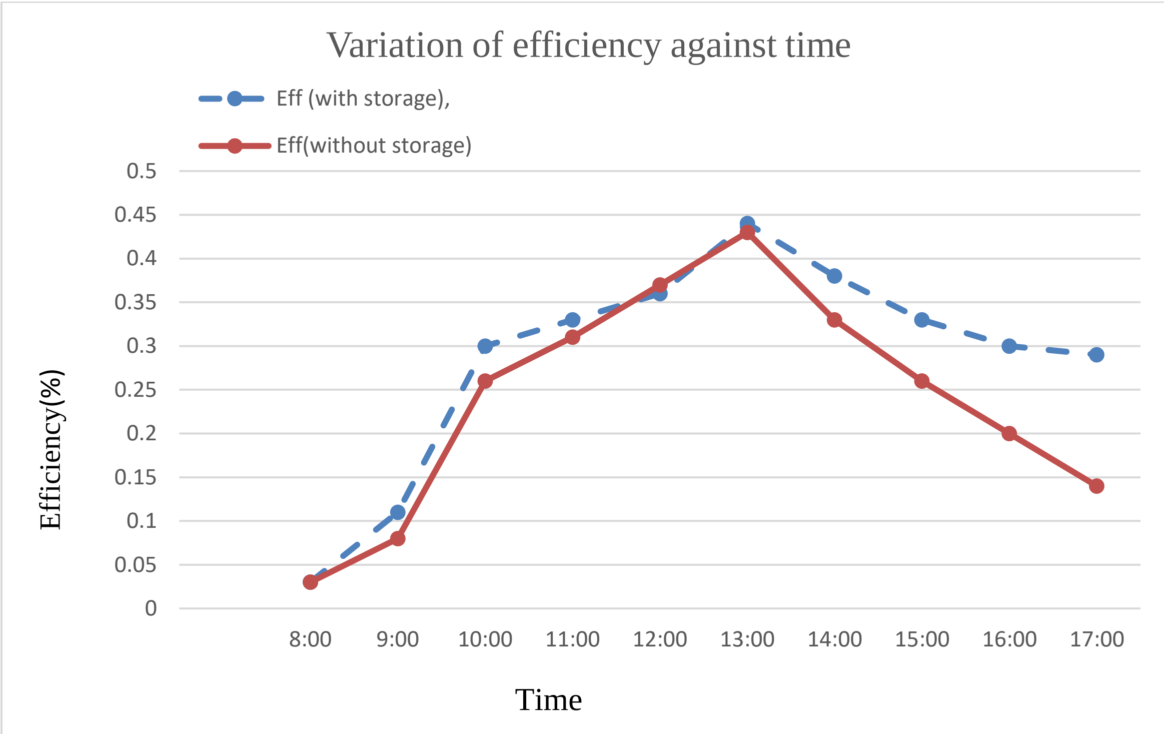

Figure 4. 7 Variation of collector efficiency with time

Figure 4.8 depicts the variation of thermal efficiency and useful heat energy leaving the collector with the beam radiation throughout the monthly average day of May 15, 2021. During the experiment, from 8:00 am to 17:00, the beam radiation varies in the range of 460 W/m^2 to 629.3 W/m^2. Most of the time, the peak value of collector temperature is observed at maximum solar intensity about solar noon. The maximum thermal efficiency was found to be 44.33% at the maximum solar radiation intensity with storage and 43% with no storage materials at 13:00. When there is no energy storing material, the maximum temperature reached by air is comparatively less and during the evening there was a high fall rate in the temperature, at that time the efficieny of the system fall with the fall of temperature.

No-load efficiency of 66.95% has been reported by[24] in natural convection solar collectors. Further, [25] have reported the thermal efficiency of flat plate collectors to be 62% at an airflow rate of 0.03 kg/m^{2}s. The instantaneous efficiency was found to be decreasing with time. The efficiency is a function of the temperature difference between plate and air as well as air and glass cover as shown in Eq. (11). With increasing time, the temperatures of the plate, air, and glass cover are also increasing; thereby, decreasing the values of (Tp-Ta) and (Ta-Tg). Again, the radiation intensity drastically reduced in the afternoon.

4.4 Candling Test Result

The percentage of fertility and hatchability of the eggs were calculated as shown in Table 4.6. The results obtained during the test show that out of 18 eggs set in the incubator 7 eggs were infertile. The percentage fertility of eggs was 61.11%. Also, out of 11 fertile eggs, 3 eggs were hatched, which resulted in a percentage hatchability of 27.27%. When compared to prior studies on incubator hatchability, the incubator was medium as the primary test. Using Tibetan and Dwarf chickens, [26] found a hatchability range of 26.23 percent–79.72 percent, whereas [27] found a hatchability range of 47 percent–76 percent using Fulani-ecotype birds. The hatchability of chicken eggs is influenced by a variety of parameters such as egg age, storage temperature, mother hen age, management and raising technique, mating method, incubation relative humidity, and egg rotation angle[28]. The eggs obtained from the farm have a high rate of infertility, which might be due to low fertility caused by the farm's frequent mating. Other issues such as incorrect mating ratios, breeder age, and poor management/social stress such as the insufficient floor, feeding, and water space, among others, maybe at work. [29].

Table 4. 6 Candling test of incubation

Candling check on the 5th day of incubation			
No of eggs	Development	Observation	Remark
2	Not visible	Clear	Infertile
5	Not visible	Large air space	Infertile
7	Visible at one end	Lines strolling across	Fertile

4	Visible on the center	Visible purple of red stains	Fertile
Candling test on the 14th day of incubation			
7	Not visible	Clear	No development
7	Dark appearance	Clear air space	Development in progress
4	The whole egg is dark	No air space	Development has ceased
Candling test on the 17th day of incubation			
2	Dark appearance	Beak is Visible	Development near completion
1	Dark appearance	Clear air space	Development in progress

4.5 Validation Result

The numerical result obtained from COMSOL Multiphysics software was validated using the data obtained by experimental investigation using statistical analysis. Figure 4.9 shows the experimental validation of the average temperature of the collector plate.

assembly for solar-powered egg incubator test. It could be seen that the temperature obtained by numerical simulation was in reasonable agreement with those measured during the experimental investigation. The indicator have been used to show the model accuracy is indicators are standard error (SE) in absorber plate temperature as follows.

$$SE = \frac{\sqrt{\sum_{i=1}^{N}(T_{exp,i} - T_{pr,i})^2}}{N-1} \quad \text{..} (4.1)$$

where: $T_{exp,i}$ and $T_{pr,i}$, are the experimented and computed (COSMOL predicted) collector outlet temperature, for the ith observation respectively, while N refers to the total number of values.

The SE with storage and without storage materials were 5.57, and 7.01 and respectively for experiment and computed (COMSOL predicted) results.

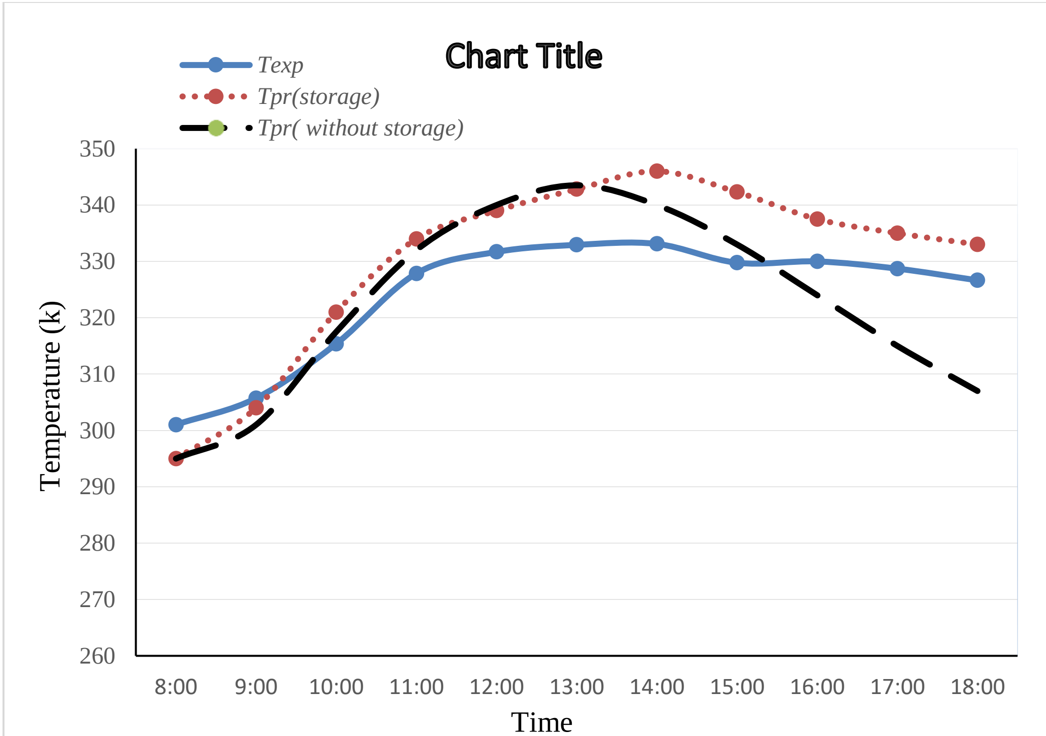

Figure 4. 8 Comparison of simulation and experimental Temperature variations of FP

CHAPTER FIVE

5. CONCLUSION AND RECOMMENDATION

5.1 Conclusion

In this present study simulation and experimental evaluation of a solar-powered egg incubator with integrated thermal energy storage for the study area was carried out. The system prototype was constructed using locally sourced materials at Bako agricultural engineering research center laboratory and tested on latitude 9.06^{o}N. The incubator is made up of a solar collector with built-in thermal storage and a 50-egg capacity incubation chamber. The first solar energy potential of the study area was assessed. There is sufficient sunlight that transformed into the energy required for a solar egg incubator by flat plate solar collector and built-in thermal energy storage in the study area. During the incubating period, there is sufficient sunlight that is converted into the energy required for a solar-powered egg incubator by a flat plate solar collector in the study area. The result showed that on the highest solar radiation days, the average outlet collector temperature was 55^{o}C and 37^{o}C was obtained on the lowest solar radiation days. The collector thermal efficiency was found to be 44.33 %. The fertility and hatchability of eggs were tested using a total of 20 eggs over 21 days in a solar-powered egg incubator. The incubating chamber was maintained by using a temperature controller (thermostat STC 1000) throughout the incubating period within a temperature range of 36.5 to 39.5^{o}C and a relative humidity range of 40 to 75 %. The percentage fertility and hatchability of eggs were 61.11% and 27.27 % respectively. In addition, the Finite element (FE) model was developed using COMSOL Multiphysics 5.4 software to study the temperature distribution inside the solar collector. The temperature distribution inside the System using COMSOL finite element analysis revealed a temperature variation of air at various locations of the solar collector, air near the absorber plate being at a higher temperature as compared to that near the glass cover. The COMSOL predicted the temperature of the air inside of the solar collector and the data obtained from the experimental investigation was close agreement validated.

5.2 Recommendation

The solar-powered egg incubator is designed and modeled in different nations of the world. But in Ethiopia, there is a limited number of incubators working with the environmental temperature. In this thesis work, I have done simulation and experimental tests of the solar-powered egg incubator integrated with the thermal energy storage system. For the future, I have recommended that Detail cost analysis with material selection for better system performance, to get monthly and hourly data values of solar radiation for the study area by horizontal flat plate, measurements need for many days repeatedly, Further analysis and biological test needed to know the characteristics of egg embryo growth, and if the system is done in a very well and organized manner taking a long time and using all the necessary materials, the project is exactly profitable and developmental.

REFERENCE

[1] E. Bala, "Design and Construction of a Fully Automated Egg Incubator Using Electric / Battery," vol. 18, no. 2, pp. 319–332, 2020.

[2] K. Shilpa, K. M. Reddy, C. H. S. Krishna, K. Vishalakshi, and P. V. Kumar, "Solar Incubator By Using Temperature Controller," pp. 1094–1106, 2020.

[3] A. Gbabo, "Design, Construction and Performance Evaluation of an Electric Powered Egg Incubator," *Int. J. Res. Eng. Technol.*, vol. 03, no. 03, pp. 521–526, 2014.

[4] FAO, *Innovative Policies and Institutions to Support AgrP-Industry Development*. 2011.

[5] J. Holewa, A. Król, and E. Kukulska-Zajac, "Biogas as an alternative to natural gas?," *Chemik*, vol. 67, no. 11, pp. 1073–1078, 2013.

[6] Kifilideen L. Osanyinpeju, Adewole A. Aderinlewo, Olayide R. Adetunji, and Emmanuel S. Ajisegiri, "Development of Solar Powered Poultry Egg Incubator," *Proc. 2016 Int. Conf. SET A Driv. force Sustain. Dev. tagged COLENG 2016, Fed. Univ. Agric. Abeokuta, March 7-11, 2016*, vol. 1, pp. 278–283, 2016.

[7] "downloadsexceeded." .

[8] A. Agboola, O. Olaniyi, and S. Aliyu, "Increasing Livestock Production in Nigeria: Development of Cost-Effective Models for Bird-Egg Incubator," *J. Emerg. …*, vol. 3, no. 3, pp. 707–716, 2013.

[9] A. Metwally, "Improving Performance of the Poultry Eggs Incubator using the Pulse Repetition Frequency," *J. Soil Sci. Agric. Eng.*, vol. 11, no. 5, pp. 151–156, 2020.

[10] P. J. Graham, P. A. Kranenburg, and C. C. Schwab, "Project Omoverhi : a thermal storage solution," 2012.

[11] K. G. Mansaray and O. Yansaneh, "Fabrication and Performance Evaluation of a Solar Powered Chicken Egg Incubator," vol. 5, no. 6, pp. 31–36, 2015.

[12] K. L. Osanyinpeju, A. A. Aderinlewo, O. R. Adetunji, and E. S. A. Ajisegiri, "Investigation of Suitable Time for the Performance Measurement and Evaluation of Mono-Crystalline Photovoltaic Panels At Federal University of Agriculture, Abeokuta (Funaab), Alabata, Ogun State, Nigeria," *Int. J. Adv. Manag. Technol. Eng. Sci. IJAMTES (ISSN NO 2249-7455)*, vol. 8, no. 4, pp. 503–522, 2018.

[13] KIFILIDEEN L. OSANYINPEJU, ADEWOLE A. ADERINLEWO, OLAYIDE R. ADETUNJI, and EMMANUEL S. A. AJISEGIRI, "Performance Evaluation of Mono-Crystalline Photovoltaic Panels in Funaab, Alabata, Ogun State, Nigeria

Weather Condition ," *Int. J. Innov. Eng. Res. Technol. [Ijiert]* , vol. 5, no. 2, pp. 8–20, 2018.

[14] J. A. D. Deceased and W. A. Beckman, *Solar engineering of thermal processes*, vol. 3, no. 3. 1982.

[15] "duffie-beckman_-_solar_engineering_of_thermal_process GOOD.pdf." .

[16] M. M. Maroneze, L. Q. Zepka, J. G. Vieira, M. I. Queiroz, and E. Jacob-Lopes, "A tecnologia de remoção de fósforo: Gerenciamento do elemento em resíduos industriais," *Rev. Ambient. e Agua*, vol. 9, no. 3, pp. 445–458, 2014.

[17] D. Ashebir, "Design numerical investigation of waste heat recovery system coupled to Electric Injera baking pans(Msc Thesis)," p. 61, 2018.

[18] A. Mahapatra and P. P. Tripathy, "Thermal performance analysis of natural convection solar dryers under no load condition: experimental investigation and numerical simulation," *Int. J. Green Energy*, vol. 16, no. 15, pp. 1448–1464, 2019.

[19] S. Liu, Y. Ogiwara, M. Fukuoka, and N. Sakai, "Investigation and modeling of temperature changes in food heated in a flatbed microwave oven," *J. Food Eng.*, vol. 131, pp. 142–153, 2014.

[20] E. O. Uzodinma, O. Ojike, U. J. Etoamaihe, and W. I. Okonkwo, "Case Studies in Thermal Engineering Performance study of a solar poultry egg incubator with phase change heat storage subsystem," *Case Stud. Therm. Eng.*, vol. 18, no. October 2019, p. 100593, 2020.

[21] B. O. Bolaji, "Design and Performance Evaluation of a Solar Poultry Egg Incubator," no. July, 2020.

[22] K. L. Osanyinpeju, A. A. Aderinlewo, E. S. A. Ajisegiri, and O. R. Adetunji, "Development of a Solar Powered Poultry Egg Incubator for South West Nigeria," *Int. J. Innov. Res. Creat. Technol. (ISSN 2454-5988)*, vol. 3, no. 6, pp. 50–63, 2018.

[23] T. Kerso and M. Village, "Energy Resource Potential Assessment for Solar Photovoltaic-Micro Hydro Hybrid Power Generation System .," vol. 5, no. 01, pp. 333–339, 2016.

[24] A. A. Gatea, "Design, construction and performance evaluation of solar maize dryer," *J. Agric. Biotechnol. Sustain. Dev.*, vol. 2, no. 3, pp. 39–46, 2010.

[25] P. Gbaha, H. Yobouet Andoh, J. Kouassi Saraka, B. Kaménan Koua, and S. Touré, "Experimental investigation of a solar dryer with natural convective heat flow," *Renew. Energy*, vol. 32, no. 11, pp. 1817–1829, 2007.

[26] L. De Smit *et al.*, "Embryonic developmental plasticity of the chick: Increased CO2

during early stages of incubation changes the developmental trajectories during prenatal and postnatal growth," *Comp. Biochem. Physiol. - A Mol. Integr. Physiol.*, vol. 145, no. 2, pp. 166–175, 2006.

[27] T. R. Fayeye, K. L. Ayorinde, V. Ojo, and O. M. Adesina, "Frequency and influence of some major genes on body weight and body size parameters of Nigerian local chickens," *Livest. Res. Rural Dev.*, vol. 18, no. 3, pp. 47–56, 2006.

[28] E. Stener-victorin, L. J. Moran, S. A. Robertson, N. K. Stepto, and R. J. Norman, "Copyright © 2019 the authors," vol. 12, no. 2, pp. 1–10, 2019.

[29] "A.M.kingori,"influence egg fertility and hatchablity in poulitry," Dept,agri.sciences. pp.483-492,2011." .

APPENDIXES

Appendix A

MATLAB code used to estimate monthly average daily and hourly, beam and diffuse solar radiation at the study area.

```
z = 1.65;               % elevation of the site above sea level
A= 0.158;              % latitude of the location
phi= 3.14;
e = 1367;               %solar constant
lst = [7,8,9,10,11,12,13,14,15,16,17,18];
y= [86.53,87.91,89.61,91.5,93.1,93.87,93.51,92.16,90.35,88.47,86.89,86.14];
l=((y-60) *pi)/180;
ns = [8.5,8.6,7.9,7.4,7.1,5.8,3.6,3.4,4.7,7.5,8.7,8.9];
decl= (([-20.92, -12.96, -2.42,9.41,18.79,23.09,21.18,13.45,4,7, -9.6, -18.91, -
        23.05]) *pi)/180;                             % declination angle
wes=(([86.53,87.91,89.61,91.5,93.1,93.87,93.51,92.16,90.35,88.47,86.89,86.14])
        *pi)/180;                                      % hour angle
n= [17,47,75,105,135,162,198,228,258,288,318,344];
   for k=1:1:12;
      w(k)=15*(12-lst(k));
      d(k)=(w(k)*pi)/180;
     Ns(k)= 2/15*y(k);
 a(k) = -0.309 + 0.539*cos(A)-0.0693*(z)+ 0.290*(ns(k)/Ns(k));
r(k) = 1.449-0.553*cos(A)- 0.694*(ns(k)/Ns(k));
f=(24*e*3600)/phi;
u(k)=(ns(k)/Ns(k));
t(k)=.409+.5016*sin(l(k));
v(k)=.6609-.4767*sin(l(k));
%e(k)=pi/24*(t(k)+v(k)*cos(d(k)));
s(k)=r(k)*u(k);
g(k)=1+.033*(cos(360*n(k)/365));
m(k)=cos(decl(k)) *cos(A)*sin(wes(k));
```

```
p(k)=((phi*wes(k))/180) *sin(A)*sin(decl(k));
Ho(k)=f*g(k)*(m(k)+p(k));
 H(k) = j(k)*(a(k)+s(k));
 Hd(k)=H(k)*(0.931-0.814*(u(k)));
q(k)=(pi/24) *(t(k)+v(k)*cos(d(k)));
qq(k)=cos(d(k))-cos(wes(k));
qqq(k)=sin(wes(k)) -(pi*y(k)/180) *cos(wes(k));
ih(k)=(q(k)*qq(k))/qqq(k);
    end
```

Metrological data

Table A.1: - Five years monthly average climatic data of the experimental area

Metrological station: Bako				Country: Ethiopia		
Altitude: 1650m.			latitude: 9^0 North	Long: 37^0 East		
Month	Min.Temp	Max.Temp	Humidity	Winds	Sun	Rad
	°C	°C	%	km/day	hours	MJ/m²/day
January	12.1	30.4	51	73	8.5	20.1
February	12.7	31.4	48	82	8.6	21.5
March	14.0	31.2	48	94	7.9	21.5
April	14.5	31.3	51	93	7.4	20.9
May	14.8	29.2	57	92	7.1	20.0
June	14.8	26.2	66	80	5.8	17.7
July	14.9	24.5	72	65	3.6	14.5
August	14.7	24.3	72	54	3.4	14.5
September	14.6	25.4	70	46	4.7	16.5
October	13.6	27.7	63	48	7.5	20.0
November	12.2	29.0	58	54	8.7	20.5
December	11.4	29.6	54	59	8.9	20.1
Average	13.7	28.4	59	70	6.8	19.0

Appendix B

Experimental Readings

Table B.1 Experimental measurements of beam radiation-based temperature

May 05,2021			
Time interval (hrs)	$T_a(^0C)$	$T_s(^0C)$	$I(w/m^2)$
8:00	20	30	430.6
9:00	19.5	36	529
10:00	21.5	43.5	570.1
11:00	23	42.2	561.2
12:00	24.5	45.5	634.5
13:00	25.6	60.1	699.7
14:00	27	63.1	651.5
15:00	26	55.3	591.6
16:00	25	43.2	511
17:00	24	35	460.7
Average			559.39
May 10,2021			
8:00	16	22	387.2
9:00	19.5	23.5	395.1
10:00	21.5	32.1	443
11:00	23	32	442.4
12:00	25	43	509.7
13:00	25.6	50	556.4
14:00	22	37	472
15:00	22.3	32	442.4
16:00	22	26	408.6
17:00	22.1	24	397.8
Average			445.46
May 15,2021			
8:00	18	38	478.2
9:00	19.5	46	529.3
10:00	21.5	52.5	570.3
11:00	23	57.2	609.9
12:00	25	58.5	613.3
13:00	25.6	60.1	629.3
14:00	27	63.1	603.1
15:00	26	55.3	514.2
16:00	25	50.6	485.1
17:00	24	35	460
Average			541.67

Table B. 2

Measured day	Time	$T_a(^0C)$	T_p (mv)	$T_p(^0C)$	T_g(mv)	$T_g(^OC)$	T_o(°C)
May 01, 2021	8:00	19	1.612	42.1	1.52	38.81	36
	9:00	19.5	2.01	48.52	1.64	41.3	37.5
	10:00	21.5	2.12	52.38	1.67	41.25	43.2
	11:00	23.5	2.43	59.56	1.72	42.67	45.3
	12:00	25	2.63	63.38	2.	49.47	56.9
	13:00	25.6	2.35	57.93	1.75	43.4	52
	14:00	28	2.023	50.12	1.68	41.69	48.6
	15:00	26	2.26	55.36	1.73	42.9	50.2
	16:00	25	2.55	62.99	1.92	47.53	53.1
	17:00	24	2.01	49.71	1.63	40.47	42.3
	18:00	23.5	1.76	43.64	1.52	37.08	38.6

	Time	$T_a(^0C)$	T_p (mv)	$T_p(^0C)$	T_g(mv)	$T_g(^OC)$	T_o(°C)
May 02, 2021	8:00	18.2	1.612	43.12	1.53	38.78	35.7
	9:00	19	2.01	49.72	1.65	40.7	37.1
	10:00	21.5	2.12	52.38	1.67	41.45	43
	11:00	23	2.43	59.86	1.73	42.67	46.3
	12:00	25.4	2.63	64.68	2.1	49.47	56
	13:00	25.6	2.35	57.93	1.75	43.4	52
	14:00	27.1	2.023	50.4	1.68	41.69	48.6
	15:00	25.8	2.26	55.76	1.73	42.9	50.2
	16:00	24	2.55	62.99	1.92	47.53	53
	17:00	23.9	2.01	49.71	1.63	40.47	41.5
	18:00	23.1	1.76	43.64	1.52	37.08	39.1

	Time	$T_a(^0C)$	T_p (mv)	$T_p(^0C)$	T_g(mv)	$T_g(^OC)$	T_o(°C)
May 03, 2021	8:00	20	1.612	43.03	1.52	37.78	35.7
	9:00	19.5	2.01	49.72	1.64	40.7	36.1
	10:00	21.5	2.12	52.38	1.67	41.45	44
	11:00	23	2.43	59.86	1.72	42.67	46.3
	12:00	25	2.63	64.68	2	49.47	56
	13:00	25.6	2.35	57.93	1.75	43.4	52
	14:00	27	2.023	50	1.68	41.69	48.6
	15:00	26	2.26	55.76	1.73	42.9	50.2
	16:00	25	2.55	62.99	1.92	47.53	53
	17:00	24	2.01	49.71	1.63	40.47	42
	18:00	23	1.76	43.64	1.52	37.08	40

	Time	$T_a(^0C)$	T_p (mv)	$T_p(^0C)$	T_g(mv)	$T_g(^OC)$	T_o(°C)
04, 2021	8:00	18.7	1.632	42.03	1.53	37.86	35.5
	9:00	19.5	2.01	49.72	1.64	40.7	37.1
	10:00	21.5	2.12	52.38	1.67	41.45	43
	11:00	23	2.43	59.86	1.72	42.67	46.3
	12:00	25	2.63	64.68	2.	49.47	56
	13:00	25.6	2.35	57.93	1.75	43.4	52
	14:00	27	2.023	50	1.68	41.69	48.6
	15:00	26	2.26	55.76	1.73	42.9	50.2
	16:00	25	2.55	62.99	1.92	47.53	54
	17:00	24	2.01	49.71	1.63	40.47	42.4
	18:00	23.1	1.76	43.64	1.52	37.08	40

	Time	Ta(0C)	Tp(mv)	Tp(^{0}C)	Tg(mv)	Tg(^{O}C)	To(°C)
	8:00	18	1.123	28.03	1.52	37.78	35
	9:00	19.5	1.31	32.72	1.64	40.7	37.1
	10:00	21.5	1.71	42.38	1.67	41.45	43
	11:00	23	2.22	54.86	1.72	42.67	46.3
05,2021	12:00	25	2.30	58.68	2	49.47	56
	13:00	25.6	2.43	59.93	1.75	43.4	52
	14:00	27	2.44	60.1	1.68	41.69	48.6
	15:00	26	2.31	56.76	1.73	42.9	50.2
	16:00	25	2.32	56.99	1.92	47.53	53
	17:00	24	2.25	55.71	1.63	40.47	42
	18:00	23.1	2.17	53.64	1.52	37.08	39.1

	Time	T_a(^{0}C)	T_p (mv)	T_p(^{0}C)	T_g(mv)	T_g(^{O}C)	T_o(°C)
06, 2021	8:00	20	1.612	40.32	1.53	38.18	35.6
	9:00	19.5	2.01	49.72	1.64	41.2	37
	10:00	21.5	2.12	52.38	1.68	42.25	43
	11:00	23	2.43	59.86	1.72	42.67	46.3
	12:00	25	2.63	64.68	2.01	49.47	56
	13:00	25.6	2.35	57.93	1.75	43.4	52
	14:00	27	2.023	50	1.68	41.69	48.6
	15:00	26	2.26	55.76	1.73	42.9	50.2
	16:00	25	2.55	62.99	1.92	47.53	53
	17:00	24.1	2.01	49.71	1.63	40.47	42
	18:00	22.9	1.77	44.51	1.54	36.51	39.8

	Time	$T_a(^0C)$	T_p (mv)	$T_p(^0C)$	T_g(mv)	$T_g(^OC)$	T_o(°C)
07/05/ 2021	8:00	20.4	1.622	42.04	1.52	37	35
	9:00	20.5	2.01	49.72	1.64	41	37
	10:00	21.8	2.12	52.38	1.67	41.45	43
	11:00	23	2.43	59.86	1.72	42.67	45.3
	12:00	25	2.63	64.68	2.01	49.47	55.9
	13:00	25.4	2.35	57.93	1.75	43.4	52
	14:00	27.1	2.023	50	1.68	41.69	48.6
	15:00	25.9	2.26	55.76	1.73	42.9	50.2
	16:00	25	2.55	62.99	1.92	47.53	53
	17:00	24	2.01	49.71	1.63	40.47	42
	18:00	22.5	1.77	43.5	1.53	37.61	40.2

	Time	$T_a(^0C)$	T_p (mv)	$T_p(^0C)$	T_g(mv)	$T_g(^OC)$	T_o(°C)
08,2021	8:00	18.9	1.612	40.03	1.52	37.63	35.3
	9:00	19.5	2.01	49.72	1.64	40.7	37.1
	10:00	21.5	2.12	52.38	1.67	41.45	43
	11:00	23	2.43	59.86	1.72	42.67	46.3
	12:00	25	2.63	64.68	1.99	49.37	56.1
	13:00	25.6	2.35	57.93	1.75	43.4	52
	14:00	27	2.023	50	1.68	41.69	48.6
	15:00	26	2.26	55.76	1.73	42.9	50.2
	16:00	25	2.55	62.99	1.92	47.53	53
	17:00	24	2.12	48.62	1.63	40.5	44
	18:00	23.1	1.76	43.64	1.52	37.08	39.1

	Time	$T_a(^0C)$	T_p (mv)	$T_p(^0C)$	T_g(mv)	$T_g(^OC)$	T_o(°C)
	8:00	19	1.612	40.03	1.52	37.78	35
	9:00	19.5	2.01	49.72	1.64	40.7	37.1
	10:00	21.5	2.12	52.38	1.67	41.45	43
	11:00	23	2.43	59.86	1.72	42.67	46.3
	12:00	25	2.63	64.68	2.02	50.47	56
09,021	13:00	25.6	2.35	57.93	1.75	43.4	52
	14:00	27	2.023	50	1.68	41.69	48.6
	15:00	26	2.26	55.76	1.73	42.9	50.2
	16:00	25	2.55	62.99	1.92	47.53	53
	17:00	24	2.01	49.71	1.63	40.47	42
	18:00	23.5	1.71	43.64	1.51	37	39

	Time interval	$Ta(^0C)$	T_p (mv)	$T_p(^0C)$	Tg(mv)	$T_g(^0C)$	T_o(°C)
	8:00	16	0.89	22	0.86	21.5	22
	9:00	19.5	1.1	27.45	0.9	22.5	25.1
	10:00	21.5	1.16	28.939	1.47	25.7	27
10,2021	11:00	23	1.76	43.64	1.52	34.84	36.2
	12:00	25	2.26	55.76	1.78	44.13	48
	13:00	25.6	1.68	41	1.59	39.49	40.1
	14:00	22	2.023	50	1.68	41.69	46
	15:00	22.3	2.26	55.76	1.73	42.9	43.8
	16:00	22	1.53	38.03	1.39	34.5	35
	17:00	22.1	1.47	36.5	1.35	33.6	34
	18:00	20	1.009	26.01	0.96	23	25.3

	Time	$T_a(^0C)$	T_p (mv)	$T_p(^0C)$	T_g(mv)	$T_g(^OC)$	T_o(°C)
11,2021	8:00	18	1.612	40.03	1.52	37.78	35
	9:00	19.5	2.01	49.72	1.64	40.7	37.1
	10:00	21.5	2.12	52.38	1.67	41.45	43
	11:00	23	2.43	59.86	1.72	42.67	46.3
	12:00	25	2.63	64.68	2	49.47	51
	13:00	25.6	2.35	57.93	1.75	43.4	52
	14:00	27.2	2.023	50	1.68	41.69	48.6
	15:00	26	2.26	55.76	1.73	42.9	50.2
	16:00	25	2.55	62.99	1.92	47.53	51
	17:00	24	2.01	49.71	1.63	40.47	42
	18:00	23	1.66	42.64	1.53	37.81	39

	Time interval	$Ta(^0C)$	Tp (mv)	$Tp(^0C)$	Tg(mv)	$Tg(^0C)$	To(°C)
12,2021	8:00	17.5	0.89	22	0.86	22.7	22.3
	9:00	19.5	1.1	27.45	0.9	23.6	25.1
	10:00	21.5	1.16	28.939	1.47	26	27
	11:00	23	1.76	43.64	1.52	34.84	36.2
	12:00	25	2.26	55.76	1.78	44.13	48
	13:00	25.6	1.68	41	1.59	39.49	40.1
	14:00	22	2.023	50	1.68	41.69	46
	15:00	22.3	2.26	55.76	1.73	42.9	43.8
	16:00	22.5	1.53	38.03	1.39	34.5	35
	17:00	22.1	1.47	36.5	1.35	33.6	34
	18:00	19	0.93	23.49	0.86	21.5	22.3

	Time	Ta(0C)	Tp (mv)	Tp(0C)	Tg(mv)	Tg(OC)	To(°C)
13,2021	8:00	18.9	1.612	40.03	1.52	37.63	36
	9:00	19.5	2.01	49.72	1.64	40.7	37
	10:00	21.5	2.12	52.38	1.67	41.45	43
	11:00	23	2.43	59.86	1.72	42.67	46.3
	12:00	25.1	2.63	64.68	1.99	49.37	56.1
	13:00	25.6	2.35	57.93	1.75	43.4	52
	14:00	26.9	2.023	50	1.68	41.69	47
	15:00	26.1	2.26	55.76	1.73	42.9	50.2
	16:00	25	2.55	62.99	1.92	47.53	54
	17:00	23.4	2.01	49.71	1.63	40.47	42.3
	18:00	23	1.76	43.64	1.52	37	40

	Time	$T_a(^0C)$	T_p (mv)	$T_p(^0C)$	T_g(mv)	$T_g(^OC)$	T_o(°C)
14,2021	8:00	18.1	1.612	41.01	1.52	38.08	35.8
	9:00	19.9	2.01	49.72	1.64	40.7	38
	10:00	22.5	2.12	52.38	1.67	41.45	43
	11:00	23	2.43	59.86	1.72	42.67	46.3
	12:00	25	2.63	64.68	2.02	52.32	56.6
	13:00	25.6	2.35	57.93	1.75	43.4	52
	14:00	27	2.023	50	1.68	41.69	48.6
	15:00	26.2	2.26	55.76	1.73	42.9	50.2
	16:00	25	2.55	62.99	1.92	47.53	53.3
	17:00	24	2.01	49.71	1.63	40.47	42.1
	18:00	24	1.81	43.61	1.52	37.08	41

	Time	$T_a(^0C)$	T_p (mv)	$T_p(^0C)$	T_g(mv)	$T_g(^OC)$	T_o(°C)
15,2021	8:00	20	1.712	48.41	1.52	37.78	35.7
	9:00	20.5	2.01	49.72	1.64	40.7	37.1
	10:00	21.5	2.12	52.38	1.67	41.45	43
	11:00	23.2	2.43	59.86	1.72	42.67	46.3
	12:00	25	2.63	64.68	2.12	53.12	56.1
	13:00	25.6	2.35	57.93	1.75	43.4	52
	14:00	27	2.023	51.5	1.68	41.69	48.6
	15:00	26	2.26	55.76	1.73	42.9	50.2
	16:00	25	2.55	62.99	1.92	47.53	53
	17:00	24	2.01	49.71	1.63	40.47	45
	18:00	23.5	1.76	44.57	1.62	38.12	43

	Time	$T_a(^0C)$	T_p (mv)	$T_p(^0C)$	T_g(mv)	$T_g(^OC)$	T_o(°C)
16,2021	8:00	17.5	1.612	40.03	1.52	37.78	36
	9:00	19.3	2.01	49.72	1.64	40.7	36.9
	10:00	21	2.12	52.38	1.67	41.45	43
	11:00	23	2.43	59.86	1.72	42.67	46.3
	12:00	25	2.63	64.68	1.98	48.47	56
	13:00	25.6	2.35	57.93	1.75	43.4	52
	14:00	27	2.023	50	1.68	41.69	48.6
	15:00	26	2.26	55.76	1.73	42.9	50.2
	16:00	25	2.55	62.99	1.92	47.53	53
	17:00	24	2.01	49.71	1.63	40.47	42
	18:00	23	1.76	43.64	1.52	37.81	38.2

	Time (hr)	Ta(0C)	Tp (mv)	Tp(0C)	Tg(mv)	Tg(OC)	To(°C)
	8:00	20	1.68	41.69	1.43	35.55	38
	9:00	19.5	2.012	49.76	1.64	40.7	47
	10:00	21.5	2.12	52.38	1.67	41.45	48.4
17,2021	11:00	23	2.43	59.86	1.72	42.67	49.3
	12:00	25	3	73.5	2.11	51.07	53
	13:00	25.6	2.75	67.56	1.75	43.4	51
	14:00	27	2.023	50	1.68	41.69	48.6
	15:00	26	2.26	55.76	1.93	47.7	45.2
	16:00	25	2.55	62.99	1.92	47.53	46.2
	17:00	24	2.01	49.71	1.63	40.47	43.7
	18:00	23.1	1.96	48.5	1.5	37.29	40.1

	Time	T_a(^{0}C)	T_p (mv)	T_p(^{0}C)	T_g(mv)	T_g(^{O}C)	T_o(°C)
	8:00	21	1.612	40.03	1.52	37.78	35
	9:00	20.5	2.01	49.72	1.64	40.7	37.1
	10:00	21.5	2.12	52.38	1.67	41.45	43
	11:00	23	2.43	59.86	1.72	42.67	46.3
18,2021	12:00	25	2.63	64.68	2.01	49.47	56.5
	13:00	25.6	2.35	57.93	1.75	43.4	52
	14:00	27	2.023	50	1.68	41.69	48.6
	15:00	26	2.26	55.76	1.73	42.9	50.2
	16:00	25	2.55	62.99	1.92	47.53	53
	17:00	24	2.01	49.71	1.63	42.41	42.9
	18:00	23	1.76	43.64	1.62	39.25	42

	Time	$T_a(^0C)$	T_p (mv)	$T_p(^0C)$	T_g(mv)	$T_g(^OC)$	T_o(°C)
19,2021	8:00	17	1.612	40.03	1.52	37.78	36.5
	9:00	18	2.01	49.72	1.64	40.7	37.5
	10:00	21.5	2.12	52.38	1.67	41.45	43.4
	11:00	23	2.43	59.86	1.72	42.67	45.9
	12:00	25	2.63	64.68	1.86	46.40	56.2
	13:00	25	2.35	57.93	1.75	43.4	52
	14:00	27.2	2.023	50	1.68	41.69	48.6
	15:00	26	2.26	55.76	1.73	42.9	50.2
	16:00	25.4	2.55	62.99	1.92	47.53	54
	17:00	24.1	2.01	49.71	1.63	40.47	42.7
	18:00	23	1.78	44.12	1.72	39.02	40.5

	Time	$T_a(^0C)$	T_p (mv)	$T_p(^0C)$	T_g(mv)	$T_g(^OC)$	T_o(°C)
20,2021	8:00	18	1.612	40.03	1.52	37.78	35
	9:00	19.5	2.01	49.72	1.64	40.7	37.1
	10:00	21.5	2.12	52.38	1.67	41.45	43
	11:00	23	2.43	59.86	1.72	42.67	46.3
	12:00	25	2.63	64.68	2	49.47	56
	13:00	25.6	2.35	57.93	1.75	43.4	52
	14:00	27	2.023	50	1.68	41.69	48.6
	15:00	26	2.26	55.76	1.73	42.9	50.2
	16:00	25	2.55	62.99	1.92	47.53	53
	17:00	24	2.01	49.71	1.63	40.47	42
	18:00	23.1	1.76	43.64	1.52	37.08	39.1

	Time	$T_a(^0C)$	T_p (mv)	$T_p(^0C)$	T_g(mv)	$T_g(^OC)$	T_o(°C)
	8:00	18.3	1.612	40.03	1.52	37.78	35
	9:00	19.5	2.01	49.72	1.64	40.7	37.1
	10:00	21.5	2.12	52.38	1.67	41.45	43
	11:00	23	2.43	59.86	1.72	42.67	46.3
21,2021	12:00	25	2.63	64.68	1.99	49.47	56
	13:00	25	2.35	57.93	1.75	43.4	52
	14:00	27	2.023	50	1.68	41.69	48.6
	15:00	26	2.26	55.76	1.73	42.9	50.2
	16:00	25	2.55	62.99	1.92	47.53	53
	17:00	24	2.01	49.71	1.63	40.47	42
	18:00	23.8	1.76	43.42	1.52	37.12	38.5

Appendix C

Table c.1 Thermo physical properties of thermal storage materials

Material	Brick	Concrete	Lime	Sand	Ballast
Thermal conductivity (w/mk^{-1})	0.731	0.721	0.731	0.721	0.725
Specific heat capacity,Cp (J/kgK^{-1})	837	655.2	837	924	680-880
Density,p(kg/m^3)	1922	1858	1446	1601	2760-2770

Table c.2 Air property tables

948
PROPERTY TABLES AND CHARTS

TABLE A–9

Properties of air at 1 atm pressure

Temp. T, °C	Density ρ, kg/m³	Specific Heat c_p J/kg·K	Thermal Conductivity k, W/m·K	Thermal Diffusivity α, m²/s	Dynamic Viscosity μ, kg/m·s	Kinematic Viscosity ν, m²/s	Prandtl Number Pr
−150	2.866	983	0.01171	4.158×10^{-6}	8.636×10^{-6}	3.013×10^{-6}	0.7246
−100	2.038	966	0.01582	8.036×10^{-6}	1.189×10^{-6}	5.837×10^{-6}	0.7263
−50	1.582	999	0.01979	1.252×10^{-5}	1.474×10^{-5}	9.319×10^{-6}	0.7440
−40	1.514	1002	0.02057	1.356×10^{-5}	1.527×10^{-5}	1.008×10^{-5}	0.7436
−30	1.451	1004	0.02134	1.465×10^{-5}	1.579×10^{-5}	1.087×10^{-5}	0.7425
−20	1.394	1005	0.02211	1.578×10^{-5}	1.630×10^{-5}	1.169×10^{-5}	0.7408
−10	1.341	1006	0.02288	1.696×10^{-5}	1.680×10^{-5}	1.252×10^{-5}	0.7387
0	1.292	1006	0.02364	1.818×10^{-5}	1.729×10^{-5}	1.338×10^{-5}	0.7362
5	1.269	1006	0.02401	1.880×10^{-5}	1.754×10^{-5}	1.382×10^{-5}	0.7350
10	1.246	1006	0.02439	1.944×10^{-5}	1.778×10^{-5}	1.426×10^{-5}	0.7336
15	1.225	1007	0.02476	2.009×10^{-5}	1.802×10^{-5}	1.470×10^{-5}	0.7323
20	1.204	1007	0.02514	2.074×10^{-5}	1.825×10^{-5}	1.516×10^{-5}	0.7309
25	1.184	1007	0.02551	2.141×10^{-5}	1.849×10^{-5}	1.562×10^{-5}	0.7296
30	1.164	1007	0.02588	2.208×10^{-5}	1.872×10^{-5}	1.608×10^{-5}	0.7282
35	1.145	1007	0.02625	2.277×10^{-5}	1.895×10^{-5}	1.655×10^{-5}	0.7268
40	1.127	1007	0.02662	2.346×10^{-5}	1.918×10^{-5}	1.702×10^{-5}	0.7255
45	1.109	1007	0.02699	2.416×10^{-5}	1.941×10^{-5}	1.750×10^{-5}	0.7241
50	1.092	1007	0.02735	2.487×10^{-5}	1.963×10^{-5}	1.798×10^{-5}	0.7228
60	1.059	1007	0.02808	2.632×10^{-5}	2.008×10^{-5}	1.896×10^{-5}	0.7202
70	1.028	1007	0.02881	2.780×10^{-5}	2.052×10^{-5}	1.995×10^{-5}	0.7177
80	0.9994	1008	0.02953	2.931×10^{-5}	2.096×10^{-5}	2.097×10^{-5}	0.7154
90	0.9718	1008	0.03024	3.086×10^{-5}	2.139×10^{-5}	2.201×10^{-5}	0.7132
100	0.9458	1009	0.03095	3.243×10^{-5}	2.181×10^{-5}	2.306×10^{-5}	0.7111
120	0.8977	1011	0.03235	3.565×10^{-5}	2.264×10^{-5}	2.522×10^{-5}	0.7073
140	0.8542	1013	0.03374	3.898×10^{-5}	2.345×10^{-5}	2.745×10^{-5}	0.7041
160	0.8148	1016	0.03511	4.241×10^{-5}	2.420×10^{-5}	2.975×10^{-5}	0.7014
180	0.7788	1019	0.03646	4.593×10^{-5}	2.504×10^{-5}	3.212×10^{-5}	0.6992
200	0.7459	1023	0.03779	4.954×10^{-5}	2.577×10^{-5}	3.455×10^{-5}	0.6974
250	0.6746	1033	0.04104	5.890×10^{-5}	2.760×10^{-5}	4.091×10^{-5}	0.6946
300	0.6158	1044	0.04418	6.871×10^{-5}	2.934×10^{-5}	4.765×10^{-5}	0.6935
350	0.5664	1056	0.04721	7.892×10^{-5}	3.101×10^{-5}	5.475×10^{-5}	0.6937
400	0.5243	1069	0.05015	8.951×10^{-5}	3.261×10^{-5}	6.219×10^{-5}	0.6948
450	0.4880	1081	0.05298	1.004×10^{-4}	3.415×10^{-5}	6.997×10^{-5}	0.6965
500	0.4565	1093	0.05572	1.117×10^{-4}	3.563×10^{-5}	7.806×10^{-5}	0.6986
600	0.4042	1115	0.06093	1.352×10^{-4}	3.846×10^{-5}	9.515×10^{-5}	0.7037
700	0.3627	1135	0.06581	1.598×10^{-4}	4.111×10^{-5}	1.133×10^{-4}	0.7092
800	0.3289	1153	0.07037	1.855×10^{-4}	4.362×10^{-5}	1.326×10^{-4}	0.7149
900	0.3008	1169	0.07465	2.122×10^{-4}	4.600×10^{-5}	1.529×10^{-4}	0.7206
1000	0.2772	1184	0.07868	2.398×10^{-4}	4.826×10^{-5}	1.741×10^{-4}	0.7260
1500	0.1990	1234	0.09599	3.908×10^{-4}	5.817×10^{-5}	2.922×10^{-4}	0.7478
2000	0.1553	1264	0.11113	5.664×10^{-4}	6.630×10^{-5}	4.270×10^{-4}	0.7539

Note: For ideal gases, the properties c_p, k, μ, and Pr are independent of pressure. The properties ρ, ν, and α at a pressure P (in atm) other than 1 atm are determined by multiplying the values of ρ at the given temperature by P and by dividing ν and α by P.

Source: Data generated from the EES software developed by S. A. Klein and F. L. Alvarado. Original sources: Keenan, Chao, Keyes, Gas Tables, Wiley, 198; and Thermophysical Properties of Matter, Vol. 3: Thermal Conductivity, Y. S. Touloukian, P. E. Liley, S. C. Saxena, Vol. 11: Viscosity, Y. S. Touloukian, S. C. Saxena, and P. Hestermans, IFI/Plenun, NY, 1970, ISBN 0-306067020-8.